J. Webster (ed.), *Wiley Encyclopedia of Electrical and Electronics Engineering*

RADAR REMOTE SENSING OF IRREGULAR STRATIFIED MEDIA

The numerous applications of radars for the detection and identification of targets and in navigation and meteorology are well known. Its uses in remotely sensing the earth environment and planetary surfaces have received much attention more recently. The problem of interpreting the radar signals from complex structures makes it necessary to develop reliable analytical solutions to a wide class of realistic models of electromagnetic scattering problems in irregular stratified media. This article deals with the evaluation of the radar cross-sections for irregular stratified models of radar targets. To this end, scattered electromagnetic fields are analyzed using a full wave approach.

To obtain full wave solutions for the electromagnetic fields scattered by irregular stratified media with rough interfaces, iterative analytical and numerical approaches are used to solve generalized telegraphists' equations developed for unbounded layered structures. Generalized telegraphists' equations for the coupled waveguide mode amplitudes were first derived for irregular waveguides with finite cross-sections by S. A. Schelkunoff. For unbounded layered structures, the complete field expansions consist of the radiation term, as well as lateral waves and guided (surface) waves of the layered medium. Exact boundary conditions are imposed at each of the rough interfaces of the irregular layered structures. The full wave solutions are applicable to layered structures with inhomogeneous medium parameters and irregular boundaries with a broad range of roughness scales. They account for specular point scattering as well as diffuse (Bragg) scattering in a unified self-consistent manner. They have been used to evaluate the like- to cross-polarized bistatic radar scatter cross-section as well as the Mueller matrix elements that relate the incident to the scattered Stokes vectors. They have also been used to derive the observed like- and cross-polarized backscatter enhancements that are attributed to double scatter. The full wave approach can be used to evaluate the near-fields as well as the far-fields excited by small-scale (including subwavelength) and large-scale fluctuations in the surface height, complex permittivity, and permeability of the irregular stratified media.

It is well established that the perturbation theory of Rice (1) can be used to correctly predict the copolarized and cross-polarized electromagnetic fields scattered by slightly rough two-dimensionally slightly rough surfaces that separate two semi-infinite media characterized by distinct electrical and magnetic properties. Perturbation theory is valid provided that the mean-square heights and slopes of the rough surfaces are of the same order of smallness; namely, $\beta = 4k^2{}_0h^2 \ll 1, \sigma^2{}_s \ll 1$, and $k_0h \approx \sigma_s$ (where k_0 is the free space electromagnetic wavenumber of the medium above the rough interface, h is the root-mean-square height, and σ_s is the root-mean-square slope of the rough surface). These analytical results, which have been extended to "tilted" slightly rough surfaces (2), have been validated experimentally and numerically (3) for both vertically and horizontally polarized excitations for arbitrary angles of incidence and scatter (general bistatic conditions).

It is also generally assumed that the physical optics approach (4) (which is based on the Kirchhoff approximations of the surface electromagnetic fields) can be used to correctly predict the scattered electromagnetic fields from two-dimensionally random rough surfaces provided that the radii of curvature of the rough surface are very large compared to wavelength (namely, $k^2{}_0\rho^2 \gg 1$, where ρ^2 is the mean-square radius of curvature) and conditions for deep phase modulation between the scattered field contributions from the stationary phase (specular) points exist (5). Implicit in the physical optics approach is the requirement that the major

contributions to the scattered fields come from regions of the rough surface that are in the vicinity of the (stationary phase) specular points on the rough surface. For this reason, for example, the single scatter physical optics approach cannot be used to correctly predict the cross-polarized fields scattered in the plane of incidence.

The physical optics approach also fails to correctly predict the polarization (vertical and horizontal) dependence of the backscatter cross sections when the surface slopes are very small even when the large radius of curvature criterion is satisfied. Thus, for perfectly conducting surfaces with very large radii of curvature, the Kirchhoff approximations for the surface current $\boldsymbol{J}_s$ ($\boldsymbol{J}_s = 2\boldsymbol{n}x\boldsymbol{H}^i$, where $\boldsymbol{n}$ is the unit vector normal to the rough surface and $\boldsymbol{H}^i$ is the magnetic field of the incident electromagnetic waves) are correctly used to predict the physical optics co-polarized fields provided that the specular points contribute significantly to the scattered fields. If, however, the mean-square slopes are very small, such that for backscatter at oblique incidence no specular points exist, the physical optics solutions fail no matter how large the radii of curvature of the rough surface.

Because of these limitations that are inherent in the two most familiar scattering theories, researchers have attempted to develop more rigorous scattering theories that can bridge the broad range of scattering problems not covered by either the perturbation theory or the physical optics approach. When the small slope and height criteria as well as the large radii of curvature criteria and conditions for deep phase modulation and specular point scattering are satisfied, the perturbation solutions and the physical optics solutions are in agreement with each other. When neither the perturbation nor the familiar physical optics solutions are individually applicable to the random rough surfaces considered (as in the case of microwave backscatter from the sea surface and the enhanced backscatter observed in controlled laboratory experiments), both the perturbation solutions and the physical optics solutions fail (6).

This has provided the motivation to develop several versions of hybrid-perturbed physical optics approaches that combine the salient features of both of these theories (2,5,7,8,9). It has also been shown that the enhanced backscatter that has been observed from very rough surfaces is due to multiple scattering (10,11,12,13). One problem with these hybrid solutions based on a two-scale surface model is that the results critically depend upon wavenumber k_d where spectral splitting is assumed to occur (8). In general, using these hybrid approaches, one cannot choose k_d such that the large-scale surface h_l and the small-scale surface h_s (that rides on the large scale surface) simultaneously satisfy the physical optics and the perturbation restrictions, respectively. It has also been shown that even when a hybrid solution is used to approximately determine the copolarized cross section through a "suitable" choice of k_d, it cannot be used to determine the cross-polarized cross section (14,15).

The full-wave solutions are not restricted to electromagnetic scattering by layered media with irregular interfaces. Scattering due to inhomogeneities in the complex electrical permittivities and magnetic permeabilities in each layer can also be accounted for in the analysis.

The full-wave solutions can also be used to determine the coupling between the radiation fields, the lateral waves, and the guided (surface) waves of the layered structures. They can be used to determine the scattered near fields as well as far fields. Both large-scale and small-scale (including subwavelength) fluctuations of the rough surface and medium parameters are accounted for in the analysis.

Schelkunoff's Generalized Telegraphists' Equations for Bounded Irregular Waveguides and the Use of Local Mode Expansions

Generalized telegraphists' equations, which are based on the use of complete expansions of the electromagnetic waves (into vertically and horizontally polarized radiation fields, lateral waves, and surface waves) as well as on the imposition of exact boundary conditions at the rough interfaces of irregular stratified media, have been derived (16,17,18) for electromagnetic fields scattered by irregular stratified media with rough interfaces. The

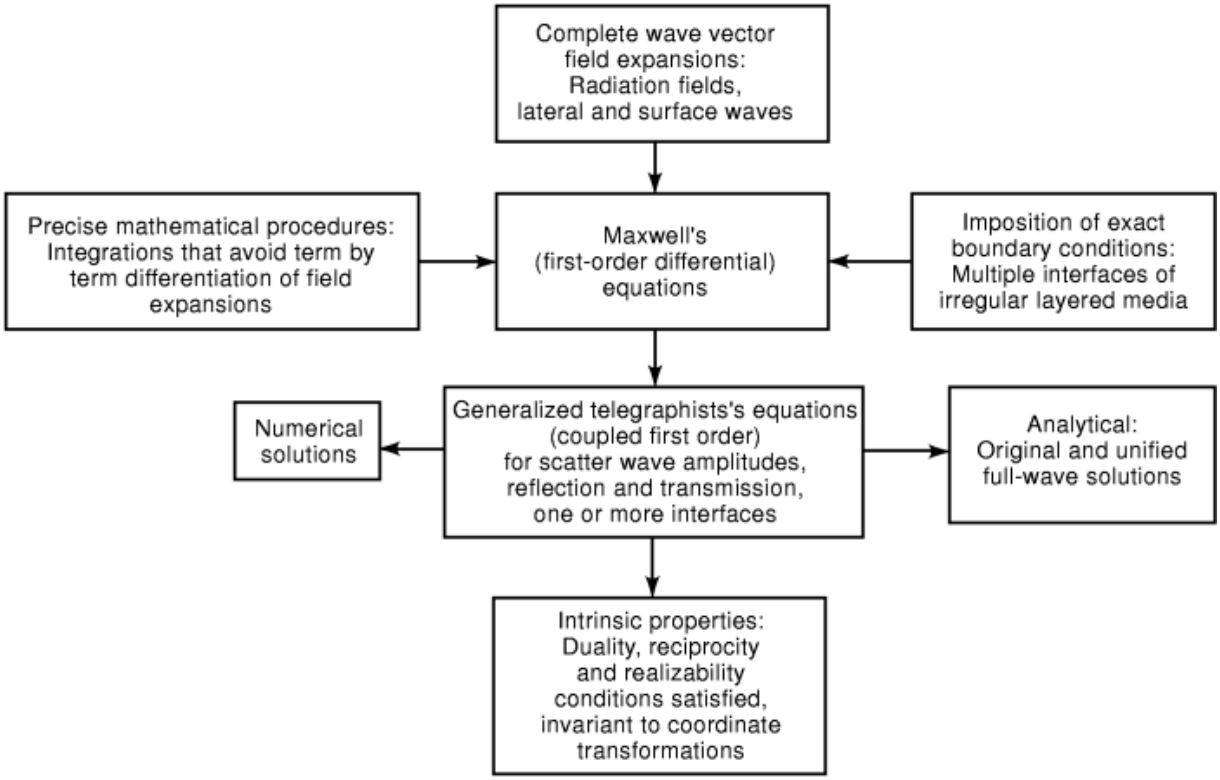

Fig. 1. Schematic of procedures for deriving the generalized telegraphists' equations.

analytical procedures used to derive these generalized telegraphists' equations are similar to those advanced by Schelkunoff (19), to solve problems of mode coupling in irregular waveguides with finite cross sections and impedance boundary conditions. Since the field expansions do not converge uniformly on the irregular boundaries, Schelkunoff (19,20) employed precise mathematical procedures to avoid term-by-term differentiation of the field expansions (infinite sets of TE and TM modes for cylindrical waveguides).

The method used to convert Maxwell's equations into sets of generalized telegraphists' equations for the reflected and transmitted wave amplitudes in irregular layered structures is shown schematically in Fig. 1. The intrinsic properties duality, reciprocity, realizability, and invariance to coordinate transformations are also listed in Fig. 1. For open structures consisting of half-spaces (such as the irregular-layered media considered in this work), the complete field expansions are associated with integrals along two branch cuts (the radiation and the lateral wave terms) and residues at pole singularities (waves guided by the stratified structure) (16,17,18).

Schelkunoff's method has also been used to solve problems of mode coupling in a wide class of irregular waveguides such as waveguide tapers and waveguide bends, as well as in waveguides with nonperfectly conducting surfaces that are characterized by impedance boundary conditions (19,20). In all these bounded waveguide systems, the field expansions are expressed in terms of infinite, discrete sets of propagating and evanescent waveguide modes associated with the characteristic equations for cylindrical waveguides with ideal, perfectly conducting boundaries. In waveguides of arbitrarily varying cross sections with finitely conducting boundaries, the modes of the ideal cylindrical waveguides, while complete, do not individually satisfy the correct boundary conditions, and the mode expansions do not uniformly converge on the irregular boundaries. To keep

his analysis rigorous, Schelkunoff (19,20), employed rather tedious, but necessary, mathematical procedures on imposing exact boundary conditions. Thus, for example, orders of integration and differentiation are not interchanged in order to account for the nonuniform convergence of the field expansions and the fact that the range of the cross section variables (limits of the corresponding integrals) are not constant. The coupling between the waveguide modes is due to the nonideal boundary conditions.

In an attempt to reduce the number of significant coupled, spurious modes that need to be accounted for in multimode waveguides with irregular cross sections, new generalized telegraphists' equations were derived based on field expansions in terms of a complete set of waveguide modes that individually satisfy the boundary conditions locally. Thus, for example, in waveguides with abrupt or gradual tapers, waveguide modes in uniform tapers (with constant flare angles) were used in the local field expansions (21,22,23). In waveguide bends with arbitrarily varying curvatures, the fields were expressed in terms of local annular waveguide modes (24,25) and in waveguides with varying impedance boundaries, modes that locally satisfy the impedance boundary conditions were used (26,27). The modal equations for the local waveguide modes were usually more difficult to solve than those for ideal cylindrical waveguides. However, the generalized telegraphists' equations can be solved numerically (using the Runge–Kutta Method) more readily when the local modal expansions are used, since coupling into the spurious local modes is bunched more tightly around the incident mode. This is because the local modes individually satisfy the local boundary conditions in the waveguide.

These analytical and numerical results were validated experimentally in a series of controlled laboratory experiments used to synthesize waveguide transition sections (28). These controlled laboratory studies were first conceived by Wait (29,30,31), to study VLF radio wave propagation in scaled laboratory models of the earth-ionosphere waveguide. In these models, the ionosphere effective boundary was simulated by an absorbing foam material with a specified complex dielectric coefficient and thickness (manufactured by Emerson Cumming) (32, 33).The earth's curvature was also simulated in these laboratory models using a nondissipative inhomogeneous dielectric material to load the interior of the straight model waveguide (34,36). This experimental procedure to stimulate curvature was carried out in the scaled model at microwave frequencies (scaling factor 10^6). It is analogous to the mathematical earth-flattening technique developed by Kerr (37). The dominant mode in the (simulated) curved model waveguide had the same characteristics of the earth-detached mode in the earth-ionosphere waveguide. They can be expressed in terms of Airy integral functions (instead of sinusoidal functions in empty, rectangular waveguides).

Generalized Telegraphists' Equations for Irregular Stratified Media with one or Two Half-Spaces

Following the extensive analytical, numerical, and experimental work on electromagnetic wave propagation in bounded irregular waveguide structures, propagation in irregular stratified structures with one or two infinite half-spaces were analyzed using the full-wave method. Approximate impedance boundary conditions (38,39) were replaced by exact boundary conditions at the rough interface between two media characterized by different complex permittivities and permeabilities (16,18). Furthermore, scattering due to laterally inhomogeneous permittivities and permeabilities in each layer of the irregular stratified media are also accounted for in the analysis.

The initial impetus for this work was the complex and intriguing sloping beach problem considered by Wait and Schlak (40) in which the sea was modeled (two-dimensionally) as a small-angle wedge region adjacent to horizontal dry land. Exact modal expansions of the fields in the four wedge-shaped regions (sea water, wet land under the sea, dry land, and free space) involve Kontorowich–Lebedev transforms (41). The relationships between the Fourier, Watson, and Kontorowich–Lebedev transforms have been obtained through the use of a generalized Bessel transforms (42). The analytical solution based on the Kontorowich–Lebedev transforms involve integration over the order of the Bessel functions. Schlak and Wait (40) employed a geometric optics approach which give exact results for parallel stratified media. However, these results were shown by them

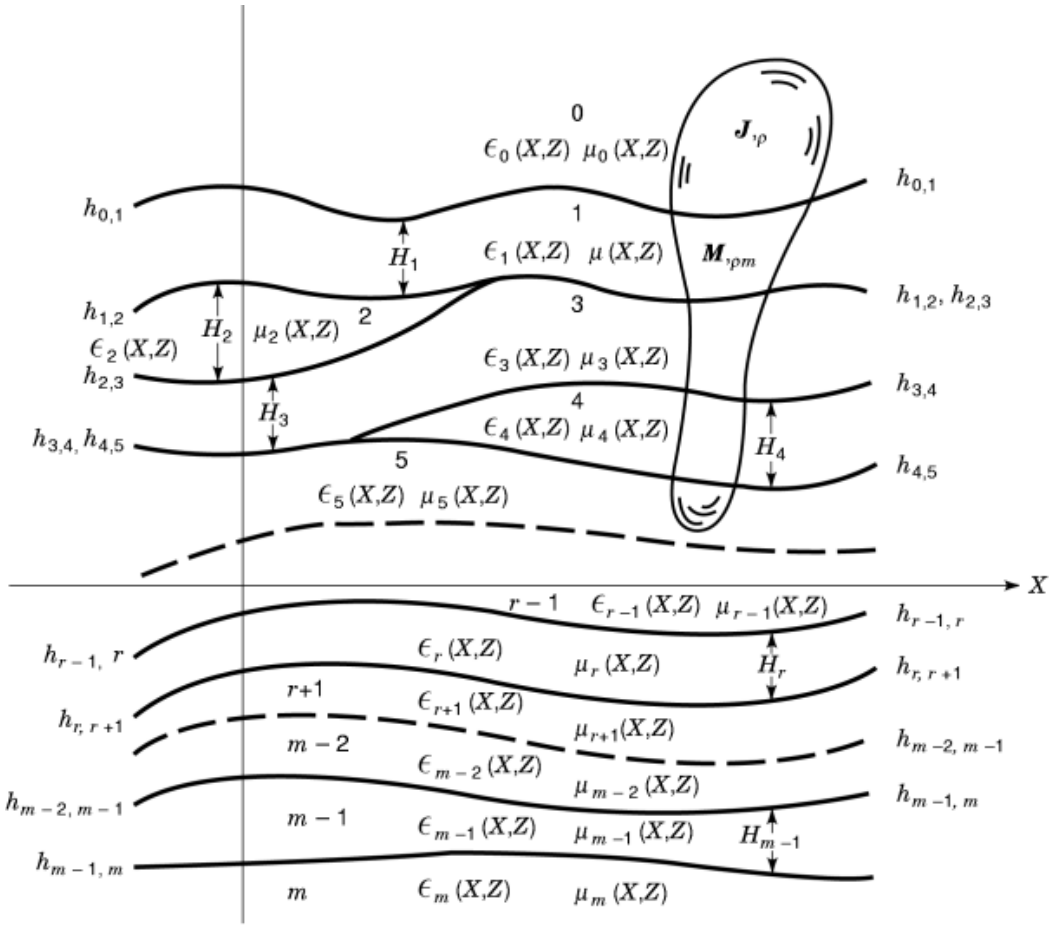

Fig. 2. Electromagnetic radiation in irregular layered structures.

to be nonreciprocal even for the small wedge angles they considered. King and Husting (43), who conducted a series of controlled experiments on laboratory models, showed that the results were more accurate when the direction of propagation was toward the apex of the wedge (rather than away from it).

Transformation of Maxwell's Equations

In this section the full-wave procedures used to convert Maxwell's equations into generalized Telegraphists' equations are outlined for propagation of electromagnetic waves in irregular layered structures with two-dimensionally rough interfaces and transversely varying electromagnetic parameters. The interested reader will find the details of the analysis in the published literature (16,17,18). The procedures are shown schematically in Fig. 1, and the irregular layered structure is illustrated in Fig. 2. The vertical axis is y and the interface between medium i and $i+1$ is given by $f(x, y, z) = y - h_{i,i+1}(x, z) = 0$. The complex permeativity ϵ and permeability μ in each layer of the structure are assumed to be functions of the lateral variables x and z.

Maxwell's equation for the transverse (y, z) components (denoted by subscript T) of the electric $\boldsymbol{E}$ and magnetic $\boldsymbol{H}$ fields can be expressed as follows:

$$-\frac{\partial \boldsymbol{E}_{\mathrm{T}}}{\partial x} = i\omega\mu(\boldsymbol{H}_{\mathrm{T}} \times \boldsymbol{a}_x) - \frac{1}{i\omega}\nabla_{\mathrm{T}}\left(\frac{1}{\epsilon}\nabla_{\mathrm{T}} \cdot (\boldsymbol{H}_{\mathrm{T}} \times \boldsymbol{a}_x)\right) + \boldsymbol{M}_{\mathrm{T}} \times \boldsymbol{a}_x + \frac{1}{i\omega}\nabla_{\mathrm{T}}\frac{J_x}{\epsilon} \tag{1}$$

and

$$-\frac{\partial \boldsymbol{H}_{\mathrm{T}}}{\partial x} = i\omega\epsilon(\boldsymbol{a}_x \times \boldsymbol{E}_{\mathrm{T}}) - \frac{1}{i\omega}\nabla_{\mathrm{T}}\left(\frac{1}{\mu}\nabla_{\mathrm{T}} \cdot (\boldsymbol{a}_x \times \boldsymbol{E}_{\mathrm{T}})\right) + \boldsymbol{a}_x \times \boldsymbol{J}_{\mathrm{T}} + \frac{1}{i\omega}\nabla_{\mathrm{T}}\frac{M_x}{\mu} \tag{2}$$

in which the operator ∇_{T} is

$$\nabla_{\mathrm{T}} = \boldsymbol{a}_y\frac{\partial}{\partial y} + \boldsymbol{a}_z\frac{\partial}{\partial z} \tag{3}$$

and the transverse vectors are

$$\boldsymbol{A}_{\mathrm{T}} = \boldsymbol{a}_y A_y + \boldsymbol{a}_z A_z \tag{4}$$

The electric and (dual) magnetic current densities are $\boldsymbol{J}$ (A/m^2) and $\boldsymbol{M}$ (V/m^2). The exact boundary conditions imposed at each of the interfaces of the irregular layered structure are the continuity of the tangential components of the electric and magnetic fields

$$[\boldsymbol{n} \times \boldsymbol{E}]_{h^-_{i-1,i}}^{h^+_{i-1,i}} = 0, \quad [\boldsymbol{n} \times \boldsymbol{H}]_{h^-_{i-1,i}}^{h^+_{i-1,i}} = 0, \qquad i = 1, \ldots m \tag{5}$$

in which $\boldsymbol{n}$ is the unit vector normal to the interfaces

$$\boldsymbol{n}_{i,i+1} = \left(-\frac{\partial h_{i,i+1}}{\partial x}, 1, -\frac{\partial h_{i,i+1}}{\partial z}\right) \Bigg/ \left[\left(\frac{\partial h_{i,i+1}}{\partial x}\right)^2 + 1 + \left(\frac{\partial h_{i,i+1}}{\partial z}\right)^2\right]^{1/2} \tag{6}$$

The full-wave, complete expansions for the vertically (V) and horizontally (H) polarized electric and magnetic fields are given in terms of the transverse basis functions

$$\boldsymbol{e}_{\mathrm{T}}^{\mathrm{V}} = Z^{\mathrm{V}}\left(\boldsymbol{a}_y\psi^{\mathrm{V}}(v, y) - \frac{\boldsymbol{a}_z i\omega}{u^2 + w^2}\frac{\partial \psi^{\mathrm{V}}(v, y)}{\partial y}\phi(w, z)\right) \tag{7}$$

$$\boldsymbol{h}_{\mathrm{T}}^{\mathrm{V}} = \boldsymbol{a}_z \psi^{\mathrm{V}}(v,y)\phi(w,z) \tag{8}$$

$$\boldsymbol{e}_{\mathrm{T}}^{\mathrm{H}} = \boldsymbol{a}_z \psi^{\mathrm{H}}(v,y)\phi(w,z) \tag{9}$$

$$\boldsymbol{h}_{\mathrm{T}}^{\mathrm{H}} = Y^{\mathrm{H}} \left(-\boldsymbol{a}_y \psi^{\mathrm{H}}(v,y) + \frac{\boldsymbol{a}_z i\omega}{u^2+w^2} \frac{\partial \psi^{\mathrm{H}}(v,y)}{\partial y} \right) \phi(w,z) \tag{10}$$

in which the y-dependent scalar basis functions ψ^{P} for the vertically ($\mathrm{P}=\mathrm{V}$) and horizontally polarized waves associated with the radiation fields, the lateral waves, and the surface waves of the layered structure are (18)

$$R_{\mathrm{P0}}^{\mathrm{D}h}\psi_0^{\mathrm{P}}(v,y) = \begin{cases} \exp(iv_0 y) + r_{\mathrm{P0}}^{\mathrm{D}h}\exp(-iv_0 y) & \text{for medium } 0 \\ \prod_{q=1}^{r}(T_{\mathrm{P}q-1}^{\mathrm{D}}/T_{\mathrm{P}q}^{\mathrm{D}})\exp(i\sum_{q=1}^{r} v_{q-1,q}h_{q-1,q}) & \\ \times[\exp(iv_r y) + R_{\mathrm{P}r}^{\mathrm{D}h}\exp(-iv_r y)] & \\ & \text{for medium } r = 1, 2, 3, \ldots, m \end{cases} \tag{11}$$

$$R_{\mathrm{P}m}^{Uh}\psi_m^{P}(v,y) = \begin{cases} \prod_{q=1}^{m-r}(T_{\mathrm{P}m+1-q}^{\mathrm{U}}/T_{\mathrm{P}m-q}^{\mathrm{UH}})\exp(i\sum_{q=1}^{m-r} v_{m-q,m+1-q}h_{m-q,m+1-q}) & \\ \times[\exp(-iv_r y) + R_{\mathrm{P}r}^{\mathrm{U}h}\exp(iv_r y)] & \\ & \text{for medium } r = 0, 1, 2, \ldots, m-1 \\ \exp(iv_0 y) + R_{\mathrm{P0}}^{\mathrm{D}h}\exp(-iv_0 y) & \\ & \text{for medium } m \end{cases} \tag{12}$$

and

$$\psi_{\mathrm{s}}^{\mathrm{P}n}(v,y) = \psi_{\mathrm{s}}^{\mathrm{P}n}(v,h_{0,1}) \begin{cases} \exp[-iv_0^n(y-h_{0,1})] & \text{for medium } 0 \\ \dfrac{1}{T_{\mathrm{P1}}^{\mathrm{DH}}}\exp(-iv_1^n h_{0,1})[\exp(iv_1^n y) + R_{\mathrm{P1}}^{\mathrm{D}h}\exp(-iv_1^n y)] & \\ & \text{for medium } 1 \\ \dfrac{1}{T_{\mathrm{P1}}^{\mathrm{DH}}}\exp(-iv_1^n h_{0,1})\prod_{q=2}^{r}(T_{\mathrm{P}q-1}^{\mathrm{D}}/T_{\mathrm{P}q}^{\mathrm{D}h}) & \\ \exp\{i\sum_{q-2}^{r} v_{q-1,q}^n h_{q-1,q}\}[\exp(iv_r^n y) + R_{\mathrm{P}r}^{\mathrm{D}h}\exp(-iv_r^n y)] & \\ & \text{for medium } r = 2, 3, \ldots, m \end{cases} \tag{13}$$

In the above equations, R and T are associated with the Fresnel reflection and transmission coefficients, v_r is the y component of the wave vector in medium r $\boldsymbol{k}_r(u, v_r, w)$, $v_{q-1,q} = v_{q-1} - v_q$, and the z-dependent scalar

function is

$$\phi(w,z) = \exp(-iwz) \tag{14}$$

The wave impedances and admittances for the vertically and horizontally polarized waves are

$$Z^v(v,y) \to Z_r^{\mathrm{V}} = (u^2+w^2)/u\omega\epsilon_r \tag{15}$$

$$Y_r^{\mathrm{H}} = (u^2+w^2)/u\omega\mu_r \tag{16}$$

The transverse components of the electric and magnetic fields are expressed completely as follows:

$$\boldsymbol{E}_{\mathrm{T}}(x,y,z) = \sum_{0} \int_{-\infty}^{\infty} [E^{\mathrm{V}}(x,v,w)\boldsymbol{e}_{\mathrm{T}}^{\mathrm{V}} + E^{\mathrm{H}}(x,v,w)\boldsymbol{e}_{\mathrm{T}}^{\mathrm{H}}]\,dw \tag{17}$$

and

$$\boldsymbol{H}_{\mathrm{T}}(x,y,z) = \sum_{v} \int_{-\infty}^{\infty} [H^{\mathrm{V}}(x,v,w)\boldsymbol{h}_{\mathrm{T}}^{\mathrm{V}} + E^{\mathrm{H}}(x,v,w)\boldsymbol{h}_{\mathrm{T}}^{\mathrm{H}}]\,dw \tag{18}$$

in which the symbol Σ_v denotes summation (integration) over the complete wave vector spectrum consisting of the radiation term and lateral waves (associated with branch cut integrals) and the waveguide modes (or bound surface waves) of the layered structure (associated with the residues at the poles of the reflection coefficients). In Eqs. (17) and (18) the scalar field transforms for the vertically (P = V) and horizontally (P = H) polarized electric and magnetic fields are

$$E^{\mathrm{P}}(x,v,w) = \int_{-\infty}^{\infty} \boldsymbol{E}_{\mathrm{T}}(v,y,z) \cdot (\boldsymbol{h}_{\mathrm{P}}^{\mathrm{T}} \times \boldsymbol{a}_x)\,dy\,dz \tag{19}$$

and

$$H^{\mathrm{P}}(x,v,w) = \int_{-\infty}^{\infty} \boldsymbol{H}_{\mathrm{T}}(x,y,z) \cdot (\boldsymbol{a}_x \times \boldsymbol{e}_{\mathrm{P}}^{\mathrm{T}})\,dy\,dz \tag{20}$$

where the complementary (reciprocal) basis functions are

$$\begin{aligned} \boldsymbol{e}_{\mathrm{V}}^{\mathrm{T}} &= Z^{\mathrm{V}}N^{\mathrm{V}}\left(\boldsymbol{a}_y\psi^{\mathrm{V}}(v,y) + \frac{\boldsymbol{a}_z iw}{u^2+w^2}\frac{\partial\psi^{\mathrm{H}}(v,y)}{\partial y}\right)\phi^c(w,z) \\ &\equiv \boldsymbol{e}_V\phi^c \end{aligned} \tag{21}$$

$$\boldsymbol{h}_{\mathrm{V}}^{\mathrm{T}} = \boldsymbol{a}_z N^{\mathrm{V}}\psi^{\mathrm{V}}(v,y)\phi^c(w,z) \equiv \boldsymbol{h}_{\mathrm{V}}\phi^c \tag{22}$$

$$\boldsymbol{e}_{\mathrm{V}}^{\mathrm{T}} = \boldsymbol{a}_z N^{\mathrm{H}} \psi^{\mathrm{H}}(v, y)\phi^c(w, z) \equiv \boldsymbol{e}_{\mathrm{H}}\phi^c \tag{23}$$

and

$$\begin{aligned}\boldsymbol{h}_{\mathrm{H}}^{\mathrm{T}} &= Y^{\mathrm{H}} N^{\mathrm{H}} \left(-\boldsymbol{a}_y \psi^{\mathrm{H}}(v, y) - \frac{\boldsymbol{a}_z iw}{u^2 + w^2} \frac{\partial \psi^{\mathrm{H}}(v, y)}{\partial y} \right) \phi^c(w, z) \\ &\equiv \boldsymbol{h}_{\mathrm{H}}\phi^c \end{aligned} \tag{24}$$

in which $\phi^c(w, z) = (1/2\pi)\exp(iwz)$ and use has been made of the biorthogonal relationships

$$\left.\begin{aligned} &\int_{-\infty}^{\infty} e_{\mathrm{T}}^{\mathrm{P}} \cdot (h_{\mathrm{Q}}^{\mathrm{T}} \times \boldsymbol{a}_x)' dy\, dz \\ &\int_{-\infty}^{\infty} h_{\mathrm{T}}^{\mathrm{Q}} \cdot (\boldsymbol{a}_x \times \boldsymbol{e}_{\mathrm{P}}^{\mathrm{T}})'\, dy\, dz \end{aligned}\right\} = \delta_{\mathrm{P,Q}} \Delta(v - v')\delta(w - w') \tag{25}$$

In Eq. (25) the Kronecker delta $\delta_{\mathrm{P,Q}}$ implies that the vertically (P, Q = V) and horizontally (P, Q = H) polarized basis functions are orthogonal. Furthermore, the Dirac delta function $\delta(w - w')$ appearing in Eq. (25) is a result of the Fourier transform completeness and orthogonality relationships:

$$\int_{-\infty}^{\infty} \phi(w, z)\phi^c(w, z_0) dw = \delta(z - z_0) \tag{26}$$

$$\int_{-\infty}^{\infty} \phi(w, z)\phi^c(w', z)\, dz = \delta(w - w') \tag{27}$$

The corresponding completeness and orthogonality relationships satisfied by the scalar basis functions ψ^{P} are

$$\begin{aligned}\delta(y - y_0) &= \textstyle\sum_v I^{\mathrm{P}} N^{\mathrm{P}} \psi^{\mathrm{P}}(v, y)\psi^{\mathrm{P}}(v, y_0) \\ &\equiv \int_{-\infty}^{\infty} I^{\mathrm{P}} N_0^{\mathrm{P}} \psi^{\mathrm{P}}(v, y)\psi_0^{\mathrm{P}}(v, y_0)\, dv_0 \\ &\quad + \int_{-\infty}^{\infty} I^{\mathrm{P}} N_m^{\mathrm{P}} \psi_m^{\mathrm{P}}(v, y)\psi_m^{\mathrm{P}}(v, y_0)\, dv_m \\ &\quad + \textstyle\sum_{n=1}^{\mathrm{N}} I^{\mathrm{P}n} \psi_s^{\mathrm{P}n}(v, y)\psi_s^{\mathrm{P}n}(v, y_0) \end{aligned} \tag{28}$$

and

$$\begin{aligned}\int_{-\infty}^{\infty} I^{\mathrm{P}} N_q^{\mathrm{P}} \psi_q^{\mathrm{P}}(v, y)\psi_r^{\mathrm{P}}(v', y)\, dy &= \Delta(v, v') \\ &= \delta_{q,r} \begin{cases} \delta(v, v'), & v' \neq v_s \\ \delta_{v,v'}, & v = v_s \end{cases} \end{aligned} \tag{29}$$

In Eqs. (28) and (29),

$$I^{\mathrm{P}} = \begin{cases} Z^{\mathrm{V}} & \mathrm{P} = \mathrm{V} \\ Y^{\mathrm{H}} & \mathrm{P} = \mathrm{H} \end{cases} \tag{30}$$

in which Z^{V} and Y^{H} are the wave impedances and admittances for the vertically and horizontally polarized waves, respectively. Furthermore, the symbol $\Delta(v, v')$ in Eqs. (25) and (29) is the product of the Kronecker delta $\delta_{q,r}$ and the Dirac delta function $\delta(v, v')$ for the radiation and lateral wave terms or the Kronecker delta $\delta_{v,v'}$ for the bound guided (surface) waves of the layered structure. Thus the radiation fields, the lateral waves, and the guided waves of the full-wave spectrum are mutually orthogonal (16,17). The radiation fields and the lateral waves are associated with branch cut integrals in the complex wave number plane [with branch points at $k = k_0$ (uppermost medium) and $k = k_m$ (lowermost medium)]. The guided waves of the layered structure are associated with the residues at the poles of the composite reflection coefficient seen from above or below the layered structure.

In this work, it is convenient to express the vertically and horizontally polarized scalar field transforms [Eqs. (19) and (20)] in terms of the vertically and horizontally polarized forward wave amplitude a^{P} and backward wave amplitude b^{P} as follows:

$$H^{\mathrm{P}} = a^{\mathrm{P}} \pm b^{\mathrm{P}} \quad \text{and} \quad E^{\mathrm{P}} = a^{\mathrm{P}} \mp b^{\mathrm{P}} \qquad \text{for } P = \begin{cases} V \\ H \end{cases} \tag{31}$$

Upon substituting the complete field transforms into the transverse components of Maxwell's equation [Eqs. (1)–(4)], making use of the biorthogonal relationships [Eq. (28)], and imposing the exact boundary conditions at each interface of the irregular layered structure [Eq. (5)], the following generalized telegraphists' equations are derived (see Fig. 1):

$$-\frac{da^{\mathrm{P}}}{dx} - iua^{\mathrm{P}} = \sum_{Q} \sum_{v'} \int_{-\infty}^{\infty} [S^{\mathrm{BA}}_{\mathrm{PQ}} a^{\mathrm{Q}} + S^{\mathrm{BB}}_{\mathrm{PQ}} b^{\mathrm{Q}}]\, dw' - A^{\mathrm{P}} \tag{32}$$

$$-\frac{db^{\mathrm{P}}}{dx} + iub^{\mathrm{P}} = \sum_{Q} \sum_{v'} \int_{-\infty}^{\infty} [S^{\mathrm{AA}}_{\mathrm{PQ}} a^{\mathrm{Q}} + S^{\mathrm{AB}}_{\mathrm{PQ}} b^{\mathrm{Q}}]\, dw' + B^{\mathrm{P}} \tag{33}$$

where A^{P} and B^{P} are associated with the source terms $\boldsymbol{J}$ and $\boldsymbol{M}$ in Eqs. (1)–(4). Furthermore, $S^{\mathrm{BA}}{}_{\mathrm{PQ}}$ and $S^{\mathrm{AB}}{}_{\mathrm{PQ}}$ are transmission scattering coefficients, while $S^{\mathrm{AA}}{}_{\mathrm{PQ}}$ and $S^{\mathrm{BB}}{}_{\mathrm{PQ}}$ are reflection scattering coefficients. These scattering coefficients vanish when the layered medium is horizontally stratified with homogeneous medium in each layer. In this case, the forward and backward wave amplitudes for the vertically and horizontally polarized waves are decoupled and analytical closed form solutions are readily obtained. However, if the rough surface height or the complex permittivities and permeabilities are functions of x and z, the wave amplitudes are coupled. In the general case, the basic functions ψ^{P} do not individually satisfy the irregular boundary conditions and the complete field expansion do not uniformally converge at the boundaries. Thus, on following precise mathematical procedures (16,17,18,19,20), the orders of integration (summation) and differentiation cannot be interchanged. As a result, the rigorous derivations of the generalized telegraphists' equations [Eqs. (32) and (33)] are rather tedious.

The intrinsic properties of the full-wave solutions are (see Fig. 1) duality, reciprocity, realizability, and invariance to coordinate transformation. All the above properties follow directly from Maxwell's equations. [(1)–(4)], and they are not a result of any additional constraints imposed on the results. A two-dimensional scalarized version of this problem has also been analyzed (44,45,46,47). When the lowermost and/or uppermost half-space is perfectly conducting or a good conducting medium, the two boundary conditions [Eq. (5)] at the lowermost (and/or uppermost) interface can be replaced by a single surface impedance boundary condition:

$$\boldsymbol{n}x\boldsymbol{E} = Z_s\boldsymbol{n}x\boldsymbol{H}x\boldsymbol{n} \qquad (34)$$

In Eq. (34) the unit vector $\boldsymbol{n}$ is normal to the interface and points into the conducting half-space. For an isotropic conducting half-space, the surface impedance Z_s is a scalar. In general, the surface impedance can be represented by a dyad. The impedance boundary condition has been used to simplify the analysis of irregular layered structures (48,49,50,51). Contributions from integrals associated with one (or two) branch cuts are eliminated when impedance boundary conditions are used.

The generalized telegraphists's equations have also been derived for irregular multilayered cylindrical structures (52,53,54,55) and irregular spherical structures (56,57,58).

For the irregular cylindrical and spherical layered structures, the complete expansions of the fields in terms of cylindrical/spherical harmonies are related to the Watson transformations (59).When the innermost regions of the cylindrical/spherical structures are highly conducting and impedance boundary conditions are used, the contribution from the continuous portion of the wave spectrum can be ignored and the solutions are expressed in terms of discrete waveguide modes (42). A set of generalized telegraphists' equations similar to Eqs. (32) and (33) have been derived for the irregular cylindrical/spherical structures (52,53,54,55,56,57,58). However, it should be noted that for the spherical case, the wave admittances/impedances and propagation coefficients for the forward and backward propagating wave amplitudes are not the same. For the spherical/cylindrical cases, solutions of the model (characteristic) equations are far more complicated, and numerical techniques have been developed to trace the loci of the complex roots of the characteristic equations (60).

These procedures have been used to solve problems of electromagnetic wave propagation in naturally occurring or man-made perturbed models of the earth-ionosphere waveguide. Experiments in controlled laboratory models (based on the pioneering work by Wait) have been conducted to validate the analytical results (29,31,34).

Iterative Solutions to the Generalized Telegraphists' Equations and Their Relationships to the Small Perturbation Solution and the Physical/Geometrical Solutions to Rough Surface Scattering

Iterative analytical procedures, as well as numerical techniques, are used to solve the generalized telegraphists' equations [Eqs. (32) and (33)] for the forward and backward wave amplitude scattered by two-dimensionally rough surfaces (see Fig. 3). An overview of the results are shown schematically in Fig. 4. The analytical procedures are dealt with first in this section. To obtain the single scatter approximations for the wave amplitudes, the expressions for the primary fields impressed upon the rough interface due to the sources are first derived from Eqs. (32) and (33) upon neglecting all the coupling terms manifested by the scattering coefficients $S^{\mathrm{BA}}{}_{\mathrm{PQ}}$. When the sources are in the far field, the primary, incident fields impressed upon the rough surface are vertically and horizontally polarized plane waves propagating in the direction of the (free space) wave vector $\boldsymbol{k}^{\mathrm{i}}{}_0 = k^{\mathrm{i}}{}_{0x}\boldsymbol{a}_x + k^{\mathrm{i}}{}_{0y}\boldsymbol{a}_y + k^{\mathrm{i}}{}_{0z}\boldsymbol{a}_z = k_0\boldsymbol{n}^i$, where $\boldsymbol{n}^i$ is a unit vector and $k_0 = \omega\sqrt{\mu_0\epsilon_0}$. Thus, the primary electric

fields impressed upon the rough surfaces are

$$\boldsymbol{E}^{\mathrm{i}} = \boldsymbol{a}^{\mathrm{P}} E_0^{\mathrm{i}} \exp[-i(k_{0x}^{\mathrm{i}} x + k_{0z}^{\mathrm{i}} z)][\exp(ik_{0y}^{\mathrm{i}} y) + R_0^{\mathrm{P}} \exp\{ik_{0y}^{\mathrm{i}}(2h - y)\}] \tag{35}$$

where $R^{\mathrm{P}}{}_0$ is the P = V, H polarized Fresnel reflection coefficient for waves incident from medium 0 (free space) upon medium 1 (see Fig. 3), and $\boldsymbol{a}^{\mathrm{P}}$ is the unit vector in (P = V) or perpendicular (P = H) to the plane of incidence. The primary fields are proportional to the local basis function $\psi^{P}{}_0(v, y)$ given by Eq. (11). The corresponding vertically or horizontally polarized field transforms and wave amplitudes are obtained using Eqs. (19), (20), and (31). In view of the biorthogonality relationships [(25)], the primary wave amplitudes are proportional to the delta functions corresponding to the polarization (Q = V, H) and direction $\boldsymbol{k}^{i}{}_0(w^{i}{}_0, v^{i}{}_0, w^{i}{}_0)$ of the incident waves. When these expressions for the primary wave amplitudes are substituted for a^{Q} and b^{Q} on the right-hand side of Eqs. (32) and (33) (with the source terms A^{P} and B^{P} suppressed) the (iterative) differential equations for single scattered wave amplitudes are obtained. The solutions for these single scatter wave amplitudes are substituted into the expressions for the field transforms [Eqs. (17) and (18)] to obtain the single scattered fields. Since both vertically and horizontally polarized incident waves are considered and both like- and cross-polarized scattered waves result from two-dimensionally rough surfaces, the results for the diffuse scattered fields are presented here in matrix notation.

$$G_{\mathrm{S}}^{\mathrm{f}} = \left(\frac{k_0}{2\pi i}\right)^2 \int_{-\infty}^{\infty}\int_{-\infty}^{\infty} S(\boldsymbol{k}', \boldsymbol{k}^{\mathrm{i}}) \exp(-i\boldsymbol{k}_0' \cdot \boldsymbol{r}) \cdot \frac{[\exp(i\boldsymbol{v}' \cdot \boldsymbol{r}_{\mathrm{s}}) - \exp(i\boldsymbol{v}' \cdot \boldsymbol{r}_{\mathrm{t}})]}{v_y'} dx_{\mathrm{s}}\, dz_{\mathrm{s}} \frac{dk_{0y}' dk_{0z}'}{k_{0x}'} \quad G^{\mathrm{i}} = G^{\mathrm{f}} - G_{\mathrm{D}}^{\mathrm{f}} \tag{36}$$

In Eq. (36)

$$G_{\mathrm{s}}^{\mathrm{f}} = \begin{bmatrix} E_{\mathrm{s}}^{\mathrm{V}} \\ E_{\mathrm{s}}^{\mathrm{H}} \end{bmatrix}, \qquad G^{\mathrm{i}} = \begin{bmatrix} E_{\mathrm{i}}^{\mathrm{V}} \\ E_{\mathrm{i}}^{\mathrm{H}} \end{bmatrix} \tag{37}$$

where $E^{\mathrm{P}}{}_{\mathrm{s}}$ and $E^{\mathrm{P}}{}_{\mathrm{i}}$ are the vertically (P = V) and horizontally (P = H) polarized components of the scattered fields and the incident waves (at the origin), respectively.

The 2×2 scattering matrix S is given by

$$S(\boldsymbol{k}', \boldsymbol{k}^{\mathrm{i}}) = 2\cos\theta_0' \cos\theta_0^{\mathrm{i}} R(\boldsymbol{k}', \boldsymbol{k}^{\mathrm{i}}) \tag{38}$$

The elements of the matrix R are

$$R^{\mathrm{VV}} = \frac{[\mu_{\mathrm{r}} C_1' C_1^{\mathrm{i}} \cos(\phi' - \phi^{\mathrm{i}}) - S_0' S_0^{\mathrm{i}}](1 - 1/\epsilon_{\mathrm{r}}) + (1 - \mu_{\mathrm{r}}) \cos(\phi' - \phi^{\mathrm{i}})}{(C_0' + \eta_{\mathrm{r}} C_1')(C_0^{\mathrm{i}} + \eta_{\mathrm{r}} C_1^{\mathrm{i}})} \tag{39}$$

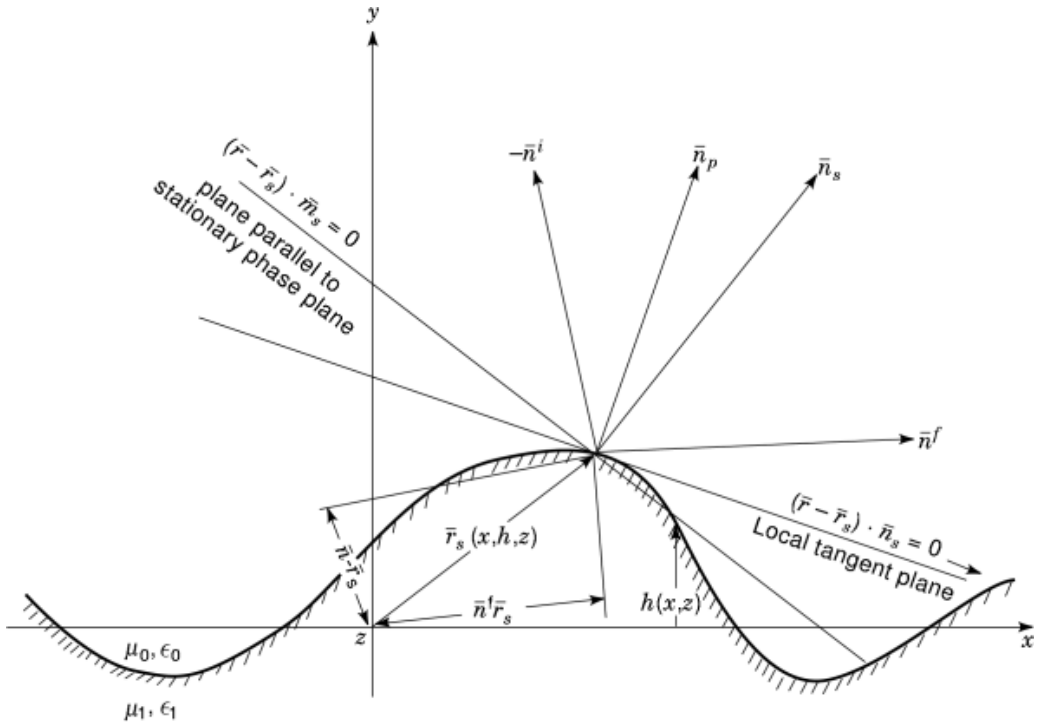

Fig. 3. Relationships between the incident and scatter wave normals $\boldsymbol{n}^{\mathrm{i}}$ and $\boldsymbol{n}^{\mathrm{f}}$, respectively, local tangent planes $(\boldsymbol{r}-\boldsymbol{r}_{\mathrm{s}})\cdot\boldsymbol{n}_{\mathrm{p}}=0$, and planes parallel to the stationary phase planes $(\boldsymbol{r}\cdot\boldsymbol{r}_{\mathrm{s}})\cdot\boldsymbol{n}_{\mathrm{s}}=0$ for rough surface scattering.

$$R^{\mathrm{HH}}=\frac{\begin{array}{r}[\epsilon_{\mathrm{r}}C_1'C_1^{\mathrm{i}}\cos(\phi'-\phi^{\mathrm{i}})-S_0'S_0^{\mathrm{i}}](1-1/\mu_{\mathrm{r}})\\ +(1-\epsilon_{\mathrm{r}})\cos(\phi'-\phi^{\mathrm{i}})\end{array}}{(C_0'+C_1'/\eta_{\mathrm{r}})(C_0^{\mathrm{i}}+C_1^{\mathrm{i}}/\eta_{\mathrm{r}})} \tag{40}$$

$$R^{\mathrm{HV}}=\frac{-\sin(\phi'-\phi^{\mathrm{i}})n_{\mathrm{r}}[(1-1/\mu_{\mathrm{r}})C_1'-(1-\epsilon_{\mathrm{r}})C_1^{\mathrm{i}}]}{(C_0'+C_1'/\eta_{\mathrm{r}})(C_0^{\mathrm{i}}+\eta_{\mathrm{r}}C_1^{\mathrm{i}})} \tag{41}$$

$$R^{\mathrm{VH}}=\frac{\sin(\phi'-\phi^{\mathrm{i}})n_{\mathrm{r}}[(1-1/\epsilon_{\mathrm{r}})C_1'-(1-\mu_{\mathrm{r}})C_1^{\mathrm{i}}]}{(C_0'+\eta_{\mathrm{r}}C_1')(C_0^{\mathrm{i}}+C_1^{\mathrm{i}}/\eta_{\mathrm{r}})} \tag{42}$$

The wave vectors in the scatter and incident directions are

$$\boldsymbol{k}_0'\equiv k_0\boldsymbol{n}'=k_0(\sin\theta_0'\cos\phi'\boldsymbol{a}_x+\cos\theta_0'\boldsymbol{a}_y+\sin\theta_0'\sin\phi'\boldsymbol{a}_z) \tag{43}$$

and

$$\boldsymbol{k}_0^{\mathrm{i}}\equiv k_0\boldsymbol{n}^{\mathrm{i}}=k_0(\sin\theta_0^{\mathrm{i}}\cos\phi^{\mathrm{i}}\boldsymbol{a}_x-\cos\theta_0^{\mathrm{i}}\boldsymbol{a}_y+\sin\theta_0^{\mathrm{i}}\sin\phi^{\mathrm{i}}\boldsymbol{a}_z) \tag{44}$$

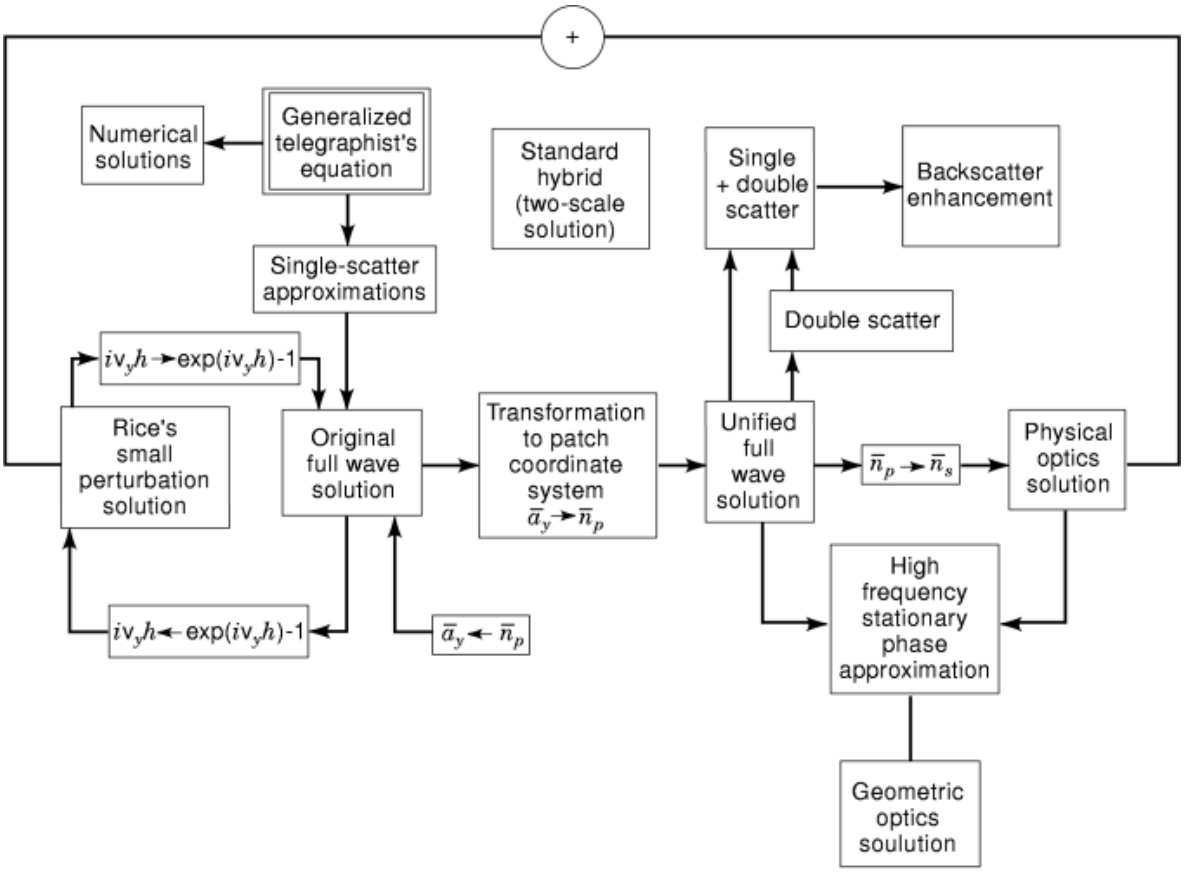

Fig. 4. Principal properties of the original and unified full-wave solutions.

where θ_0 is the elevation angle (measured from the y axis and ϕ is the azimuth angle measured from the x axis. Furthermore, $C^{\mathrm{i}}{}_0 = \cos\theta^{\mathrm{i}}{}_0$, $C'_0 = \cos\theta'_0$, $S^{\mathrm{i}}{}_0 = \sin\theta^{\mathrm{i}}{}_0$, $S'_0 = \sin\theta'_0$. The corresponding quantities associated with medium 1 are denoted by the subscript 1 and θ_1, is related to θ_0 by Snell's law. The vector $\boldsymbol{v}'$ is

$$\boldsymbol{v}' = \boldsymbol{k}_0 - \boldsymbol{k}'_0 = v'_x \boldsymbol{a}_x + v'_y \boldsymbol{a}_y + v'_z \boldsymbol{a}_z \tag{45}$$

and $\boldsymbol{r}_{\mathrm{s}}$ and $\boldsymbol{r}$ are position vectors from the origin to points on the rough surfaces and to the observation point, respectively:

$$\boldsymbol{r}_{\mathrm{s}} = x_{\mathrm{s}} \boldsymbol{a}_x + h \boldsymbol{a}_y + z_{\mathrm{s}} \boldsymbol{a}_z \tag{46}$$

$$\boldsymbol{r} = x\boldsymbol{a}_x + y\boldsymbol{a}_y + z\boldsymbol{a}_z = r\boldsymbol{n}^{\mathrm{f}} \tag{47}$$

Furthermore,

$$\boldsymbol{r}_{\mathrm{t}} = x_s \boldsymbol{a}_x + z_s \boldsymbol{a}_z = \boldsymbol{r}_{\mathrm{s}} - h\boldsymbol{a}_y \tag{48}$$

In Eq. (36) the integrations are over the rough surface (transverse) variables x_{s} and z_{s} as well as the wave vector variables k'_y and k'_z. The first term G^{f} contains the exponent $\exp(iv_y h)$ while the second term $G^{\mathrm{f}}{}_{\mathrm{d}}$ does not. On integrating the second term with respect to x_{s} and z_{s}, the delta functions are obtained:

$$\delta(k'_{0x} - k^{\mathrm{i}}_{0x}) = \frac{1}{2\pi} \int_{-\infty}^{\infty} \exp(iv'_x x_{\mathrm{s}})\, dx_{\mathrm{s}} \tag{49}$$

$$\delta(k'_{0z} - k^{\mathrm{i}}_{0z}) = \frac{1}{2\pi} \int_{-\infty}^{\infty} \exp(iv'_z z_{\mathrm{s}})\, dz_{\mathrm{s}} \tag{50}$$

Thus the second term $G^{\mathrm{f}}{}_{\mathrm{d}}$ can be readily shown to be the specularly reflected wave from a flat surface at $y = 0$, since R^{VV} and R^{HH} reduce to the Fresnel reflection coefficients for the vertically and horizontally polarized waves and $R^{\mathrm{VH}} \to 0$, $R^{\mathrm{HV}} \to 0$ for the specular case $\boldsymbol{k}' \to \boldsymbol{k}^{\mathrm{s}} = \boldsymbol{k}^{\mathrm{i}} + 2k_0 \cos\theta^{\mathrm{i}}{}_0 \boldsymbol{a}_y$, $\boldsymbol{v} \to 2k_0 \cos\theta^{\mathrm{i}}{}_0 \boldsymbol{a}_y$.

Note that the results in Eq. (36) are in complete agreement with the earlier work in which it is assumed that the vector $\boldsymbol{n}$ normal to the rough surface is restricted to the xy plane ($h_z = 0$) (25). This is because the restriction does not constrain the unit vector $\boldsymbol{n}$ to lie in the scatter plane (normal to $\boldsymbol{k}' x \boldsymbol{k}^{\mathrm{i}}$).

In the recent work by Collin (61), the author uses a different full-wave approach to the problem of scattering of plane waves from perfectly conducting surfaces: He uses a pair of odd and even scalar basis functions for the Dirichlet and Neumann boundary conditions. These basis functions and the corresponding reciprocal basis functions (chosen to be their complex conjugates) are explicit functions of y and implicit functions of x and z [through the expression for $h(x, z)$, the rough surface height]. The resulting source free wave equation is further (Fourier) transformed in x and z to obtain an equation with a dyadic operator for the vector field transform (and equivalent, slope-dependent sources that account for scattering) rather than generalized telegraphists' equations for the scalar wave amplitude. Upon inverting the dyadic operator, evaluating the residue at k_0, and integrating by parts, Collin's results are also shown to be in complete agreement with the full-wave results for the perfectly conducting case ($|\epsilon_{\mathrm{r}}| \to \infty$, $\mu_{\mathrm{r}} = 1$). Collin referred to the results for the diffuse scattered fields (25) as the original full-wave solutions (see Fig. 4).

The above first-order iterative solutions for the single scattered fields [Eq. (36)] are restricted to rough surfaces with small mean-square slopes $\sigma_{\mathrm{s}} < 0.1$ (3). This is because the scattering coefficients $S^{\alpha\beta}{}_{\mathrm{PQ}}(\alpha, \beta = \mathrm{A}, \mathrm{B})$ appearing in the generalized telegraphists' equations [Eqs. (32) and (33)] are explicitly dependent on the slopes of the rough surface. Alternatively, in Collin's work, the equivalent source terms are slope-dependent. However, unlike the small perturbation solution, the full-wave solutions are not restricted to rough surfaces with small mean-square heights. Furthermore, the full-wave solutions [Eq. (36)] can be used to evaluate the near fields, the far fields, and the fields in the intermediate region. Thus, this work can be applied to probing subwavelength structures, an area that has attracted much interest in near field optics. In addition, the first-order scattering results can be extended to multiple scattering. In particular, the full-wave approach has been used to account for double scatter that is associated with observed backscatter enhancement (12).

When the observation point is at a very large distance from the rough surfaces ($k_1 r \gg k_0 L \gg 1$ and $k_0 r \gg k_0 l \gg 1$), the integration with respect to the scatter wave vector variables (k'_{0y}, k'_{0z}) can be performed

analytically using the stationary phase method. Thus, if the observation point is in the direction

$$\boldsymbol{n}^{\mathrm{f}} = \boldsymbol{r}/|\boldsymbol{r}| = \sin\theta_0^{\mathrm{f}}\cos\phi^{\mathrm{f}}\boldsymbol{a}_x + \cos\theta_0^{\mathrm{f}}\boldsymbol{a}_y + \sin\theta_0^{\mathrm{f}}\sin\phi^{\mathrm{f}}\boldsymbol{a}_z \qquad (51)$$

the diffuse far fields scattered from the rough surface are

$$\begin{aligned} G_{\mathrm{S}}^{\mathrm{f}} &= G_0 \int_{-l}^{l}\int_{-L}^{L} S(\boldsymbol{k}^{\mathrm{f}}, \boldsymbol{k}^{\mathrm{i}})[\exp(i\boldsymbol{v}\cdot\boldsymbol{r}_{\mathrm{s}}) - \exp(i\boldsymbol{v}\cdot\boldsymbol{r}_{\mathrm{t}})]\cdot dx_{\mathrm{s}}\, dz_{\mathrm{s}} G^{\mathrm{i}} \\ &= G^{\mathrm{f}} - G_{\mathrm{D}}^{\mathrm{f}} \end{aligned} \qquad (52)$$

The expression for $S(\boldsymbol{k}^{\mathrm{f}}, \boldsymbol{k}^{\mathrm{i}})$ in Eq. (52) is the same as the expression for $S(\boldsymbol{k}', \boldsymbol{k}^{\mathrm{i}})$ in Eq. (36) except that the scatter wave vector $\boldsymbol{k}'$ is replaced by $\boldsymbol{k}^{\mathrm{f}}$, where $\boldsymbol{k}^{\mathrm{f}}{}_0 = k_0\boldsymbol{n}^{\mathrm{f}}$ [Eq. (51)] and $\boldsymbol{k}^{\mathrm{f}}{}_1$ the wave vector for $y < h(x_{\mathrm{s}}, z_{\mathrm{s}})$ is related to $\boldsymbol{k}^{\mathrm{f}}{}_0$ through Snell's law. Furthermore,

$$\boldsymbol{v} = k_0(\boldsymbol{n}^{\mathrm{f}} - \boldsymbol{n}^{\mathrm{i}}) = v_x\boldsymbol{a}_x + v_y\boldsymbol{a}_y + v_z\boldsymbol{a}_z \qquad (53)$$

and

$$G_0 = k_0^2 \exp(-ik_0 r)/2\pi i v_y r \qquad (54)$$

In Eq. (54), $v_y = k_0(C^{\mathrm{i}}{}_0 + C^{\mathrm{f}}{}_0) = k_0(\cos\theta^{\mathrm{i}}{}_0 + \cos\theta^{\mathrm{f}}{}_0)$. When the integrations with respect to x_{s} and z_{s} are performed, the term $G^{\mathrm{f}}{}_{\mathrm{D}}$ is shown to be the flat-surface quasi-specular (zero-order) scattered field which is proportional to $(4Ll/v_xLv_zl)\sin v_xL \sin v_zl$. The expression for the quasi-specular scatter term $G^{\mathrm{f}}{}_{\mathrm{D}}$ is the same as the expression for the total field G^{f} except that $\boldsymbol{r}_{\mathrm{s}}$ in G^{f} is replaced by $\boldsymbol{r}_{\mathrm{t}}$ in $G^{\mathrm{f}}{}_{\mathrm{D}}$ [Eq. (52)]. Thus, for $h(x_{\mathrm{s}}, z_{\mathrm{s}}) = 0$, they are identical and $G^{\mathrm{f}}{}_{\mathrm{s}} = 0$.

It is readily shown that the full wave-solution [Eq. (52)] reduces to the small-height–small-slope perturbation solution of Rice provided that it is assumed that $k_0 h \ll 1$. Thus on retaining the first two terms of the Taylor series expansion of $\exp(iv_y h)$ it follows that

$$\exp(i\boldsymbol{v}\cdot\boldsymbol{r}_{\mathrm{s}}) - \exp(i\boldsymbol{v}\cdot\boldsymbol{r}_{\mathrm{t}}) \approx iv_y h(x,z)\exp(i\boldsymbol{v}\cdot\boldsymbol{r}_{\mathrm{t}}) \qquad (55)$$

In this small-height–small-slope limit, the full-wave solution is indistinguishable from the small perturbation solution for the far fields scattered by slightly rough surfaces (see Fig. 3). These limiting forms of the full-wave solutions are, however, no longer invariant to coordinate transformations since $h(x, z)$ does not appear in the exponent. Furthermore, it is shown that they are valid only if the height and slopes are of the same order of smallness.

Turning now to the high-frequency limit, it is assumed that the radii of curvature of the rough surfaces are very large compared to wavelength. The unit vector $\boldsymbol{n}_{\mathrm{p}}$ normal to these large-scale patches of rough surfaces is assumed to have arbitrary orientation. Thus the planes of incidence and scatter with respect to the reference coordinate system (normal to $\boldsymbol{n}^{\mathrm{i}}x\boldsymbol{a}_y$ and $\boldsymbol{n}^{\mathrm{f}}x\boldsymbol{a}_y$, respectively) are not the same as the local planes of incidence and scatter with respect to the local coordinate system (normal to $\boldsymbol{n}^{\mathrm{i}}x\boldsymbol{n}_p$ and $\boldsymbol{n}^{\mathrm{f}}x\boldsymbol{n}_p$, respectively). Furthermore, the sines and cosines of the angles of incidence and scatter appearing in the scattering coefficients [Eqs. (39)–(42)] are not the same as the sines and cosines of the local angles of incidence and scatter. In order to account for the arbitrary slope of the large-scale surface, the surface element scattering matrix $S(\boldsymbol{k}^{\mathrm{f}}, \boldsymbol{k}^{\mathrm{i}})$ in Eq. (36) is

replaced by

$$S(\boldsymbol{k}^{\mathrm{f}}, \boldsymbol{k}^{\mathrm{i}}) \rightarrow T^{\mathrm{f}} S_{\mathrm{n}}(\boldsymbol{k}^{\mathrm{f}}, \boldsymbol{k}^{\mathrm{i}}) T^{\mathrm{i}} \equiv D(\boldsymbol{k}^{\mathrm{f}}, \boldsymbol{k}^{\mathrm{i}}) \tag{56}$$

In Eq. (56) the matrix operator T^{i} decomposes the waves which are vertically and horizontally polarized with respect to the reference plane of incidence (normal to $\boldsymbol{n}^{\mathrm{i}} x \boldsymbol{a}_y$) into vertically and horizontally polarized waves with respect to the local plane of incidence (normal to $\boldsymbol{n}^{\mathrm{i}} x \boldsymbol{n}$). Similarly, the matrix operator T^{f} decomposes the waves which are vertically and horizontally polarized with respect to the local plane of scatter (normal to $\boldsymbol{n}^{\mathrm{f}} x \boldsymbol{n}$) back into vertically and horizontally polarized waves with respect to the reference plane of scatter (normal to $\boldsymbol{n}^{\mathrm{f}} x \boldsymbol{a}_y$). Thus if ψ and ϕ are the angles between the reference and local planes of incidence and the reference and local planes of scatter, respectively, then

$$T^{\mathrm{i}} = \begin{pmatrix} C_{\psi}^{\mathrm{i}} & S_{\psi}^{\mathrm{i}} \\ -S_{\psi}^{\mathrm{i}} & C_{\psi}^{\mathrm{i}} \end{pmatrix}, \qquad T^{\mathrm{f}} \begin{pmatrix} C_{\psi}^{\mathrm{f}} & -S_{\psi}^{\mathrm{f}} \\ S_{\psi}^{\mathrm{f}} & C_{\psi}^{\mathrm{f}} \end{pmatrix} \tag{57}$$

in which for j = i or f we have

$$\begin{aligned} C_{\psi}^{\mathrm{j}} &= \cos\psi^{\mathrm{j}} \\ &= \frac{(\boldsymbol{n}^{\mathrm{j}} x \boldsymbol{a}_y) \cdot (\boldsymbol{n}^{\mathrm{j}} x \boldsymbol{n}_{\mathrm{p}})}{|\boldsymbol{n}^{\mathrm{j}} x \boldsymbol{a}_y| |\boldsymbol{n}^{\mathrm{j}} x \boldsymbol{n}_p|} \\ &= \frac{\boldsymbol{a}_y \cdot \boldsymbol{n}_{\mathrm{p}} - (\boldsymbol{n}^{\mathrm{j}} \cdot \boldsymbol{a}_y)(\boldsymbol{n}^{\mathrm{j}} \cdot \boldsymbol{n}_{\mathrm{p}})}{|\boldsymbol{n}^{\mathrm{j}} x \boldsymbol{a}_y| |\boldsymbol{n}^{\mathrm{j}} x \boldsymbol{n}_{\mathrm{p}}|} \\ &= \frac{\cos\gamma - C_0^{\mathrm{j}} C_0^{\mathrm{jn}}}{S_0^{\mathrm{j}} S_0^{\mathrm{jn}}} \end{aligned} \tag{58}$$

$$\begin{aligned} S_{\psi}^{\mathrm{j}} &= \sin\psi^{\mathrm{j}} \\ &= \frac{(\boldsymbol{n}^{\mathrm{j}} x \boldsymbol{a}_y) x (\boldsymbol{n}^{\mathrm{j}} x \boldsymbol{n}_{\mathrm{p}}) \cdot \boldsymbol{n}^{\mathrm{j}}}{|\boldsymbol{n}^{\mathrm{j}} x \boldsymbol{a}_y| |\boldsymbol{n}^{\mathrm{j}} x \boldsymbol{n}_p|} \\ &= \frac{[\boldsymbol{n}^{\mathrm{j}} \boldsymbol{a}_y \boldsymbol{n}_{\mathrm{p}}]}{|\boldsymbol{n}^{\mathrm{j}} x \boldsymbol{a}_y| |\boldsymbol{n}^{\mathrm{j}} x \boldsymbol{n}_{\mathrm{p}}|} \\ &= \frac{\sin\gamma \sin(\delta - \phi^{j})}{S_0^{\mathrm{jn}}} \end{aligned} \tag{59}$$

where

$$\boldsymbol{n}_{\mathrm{p}} = \sin\gamma \cos\delta \boldsymbol{a}_x + \cos\gamma \boldsymbol{a}_y + \sin\gamma \sin\delta \boldsymbol{a}_z \tag{60}$$

Furthermore, the cosines of the local angles of incidence and scatter appearing in $S_{\mathrm{n}}(\boldsymbol{k}^{\mathrm{f}}, \boldsymbol{k}^{\mathrm{i}})$ [Eq. (56)] are given by

$$C_0^{\mathrm{in}} = -\boldsymbol{n}^{\mathrm{i}} \cdot \boldsymbol{n}_{\mathrm{p}}, \qquad C_0^{\mathrm{fn}} = \boldsymbol{n}^{\mathrm{f}} \cdot \boldsymbol{n}_{\mathrm{p}} \tag{61}$$

while $S^{\text{in}}{}_0$ and $S^{\text{fn}}{}_0$ are the sines of the local angles of incidence and scatter. The corresponding quantities associated with medium 1 are denoted by the subscript 1. The local angles of incidence and scatter in medium 1 are related to the local angles of incidence and scatter in medium 0 through Snell law. Implicit in Eq. (56) are the self-shadow functions $U(\boldsymbol{n}^{\text{f}} \cdot \boldsymbol{n}_{\text{p}})$ and $U(-\boldsymbol{n}^{\text{i}} \cdot \boldsymbol{n}_{\text{p}})$ (where U is the unit step function) since the local angles of incidence and scatter are less than 90°. Furthermore, $\cos(\phi^{\text{f}} - \phi^{\text{i}})$ and $\sin(\phi^{\text{f}} - \phi^{\text{i}})$ appearing in Eq. (38) are replaced by (62)

$$\begin{aligned}\cos(\phi^{\text{fn}} - \phi^{\text{in}}) &= \frac{(\boldsymbol{n}^{\text{f}} x \boldsymbol{n}_{\text{p}}) \cdot (\boldsymbol{n}^{\text{i}} x \boldsymbol{n}_{\text{p}})}{|\boldsymbol{n}^{\text{f}} x \boldsymbol{n}_{\text{p}}||\boldsymbol{n}^{\text{i}} x \boldsymbol{n}_{\text{p}}|} \\ &= \frac{\boldsymbol{n}^{\text{i}} \cdot \boldsymbol{n}^{\text{f}} - (\boldsymbol{n}^{\text{f}} \cdot \boldsymbol{n}_{\text{p}})(\boldsymbol{n}^{\text{i}} \cdot \boldsymbol{n}_{\text{p}})}{S_0^{\text{fn}} S_0^{\text{in}}} \\ &= \frac{C_0^{\text{fn}} C_0^{\text{in}} - C_0^{\text{i}} C_0^{\text{f}} + S_0^{\text{i}} S_0^{\text{f}} \cos(\phi^{\text{f}} - \phi^{\text{i}})}{S_0^{\text{fn}} S_0^{\text{in}}} \end{aligned} \tag{62}$$

$$\begin{aligned}\sin(\phi^{\text{fn}} - \phi^{\text{in}}) &= \frac{(\boldsymbol{n}^{\text{f}} x \boldsymbol{n}_{\text{p}}) x (\boldsymbol{n}^{\text{i}} x \boldsymbol{n}_{\text{p}}) \cdot \boldsymbol{n}_{\text{p}}}{|\boldsymbol{n}^{\text{f}} x \boldsymbol{n}_{\text{p}}||\boldsymbol{n}^{\text{i}} x \boldsymbol{n}_{\text{p}}|} = \frac{[\boldsymbol{n}^{\text{f}} \boldsymbol{n}^{\text{i}} \boldsymbol{n}_{\text{p}}]}{S_0^{\text{fn}} S_0^{\text{in}}} \\ &= [\sin\gamma \{\cos\theta_0^{\text{i}} \sin\theta_0^{\text{f}} \sin(\phi^{\text{f}} - \delta) \\ &\quad + \cos\theta_0^{\text{f}} \sin\theta_0^{\text{i}} \sin(\phi^{\text{i}} - \delta)\} \\ &\quad + \cos\gamma \sin\theta_0^{\text{f}} \sin\theta_0^{\text{i}} \sin(\phi^{\text{f}} - \phi^{\text{i}})]/S_0^{\text{fn}} S_0^{\text{in}} \end{aligned} \tag{63}$$

The above changes represented by Eq. (56) constitutes the transformation into the large-scale (patch) coordinate system (see Fig. 5). It is readily shown that at high frequencies, the major contributions come from the vicinity of the stationary-phase, specular points on the rough surface where $\boldsymbol{n}_{\text{p}}$ is along the bisector between $\boldsymbol{n}^{\text{f}}$ and $-\boldsymbol{n}^{\text{i}}$ (see Fig. 3). Pursuant to the transformation Eq. (56) it can be shown that at these stationary-phase points, R^{VV} and R^{HH} reduce to the familiar Fresnel reflection coefficients while the cross-polarized terms R^{VH} and R^{HV} vanish at the specular points. Thus in these limits, the full-wave solution [Eq. (52)] reduces to the physical optics solution for the diffuse scattered fields (4). If, in addition, Eq. (52) is evaluated analytically using stationary-phase approximations, the full-wave solution reduces to the geometric optics solution (see Fig. 4). However, in order to account for multiple scatter at the same rough surface, it is necessary to return to the original form [Eq. (36)] even at high frequencies (13).

Full-Wave Solutions for the Radar Cross Sections for Multiple-Scale Rough Surfaces

The normalized bistatic radar cross sections σ^{PQ} for two-dimensionally rough surfaces are dependent on the polarizations of the scattered (first superscript P = V, H) and incident (second superscript Q = V, H) waves. It is defined as the following dimensionless quantity that depends on the incident and scatter wave-vector directions:

$$\sigma^{\text{PQ}}(\boldsymbol{k}^{\text{f}}, \boldsymbol{k}^{\text{i}}) = \frac{|E_{\text{S}}^{\text{P}}|^2}{|E_{\text{i}}^{\text{Q}}|} \frac{4\pi r^2}{A_{\text{y}}} \tag{64}$$

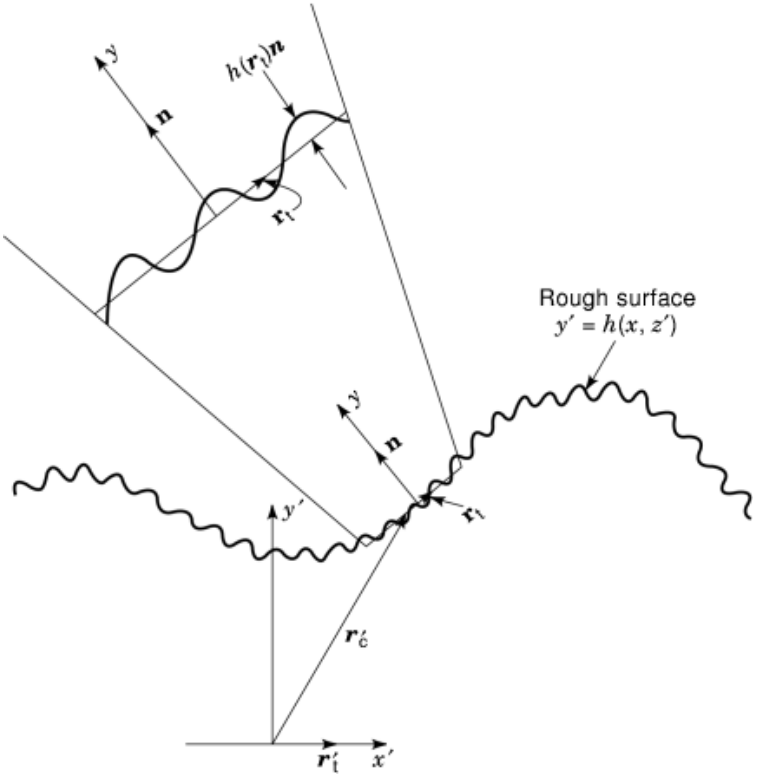

Fig. 5. Arbitrarily oriented patch of a rough surface.

In Eq. (64) the area A_y is the radar footprint, r is the distance from the rough surface to the far-field observation point. When the rough-surface statistical characteristics are homogeneous though not necessarily isotropic, the (ensemble average) full-wave radar cross section based on the original (denoted by subscript 0) full-wave analysis [Eq. (52)] is expressed as follows:

$$\langle \sigma_0^{\mathrm{PQ}} \rangle = |S^{\mathrm{PQ}}(\boldsymbol{n}^{\mathrm{f}}, \boldsymbol{n}^{\mathrm{i}})|^2 Q(\boldsymbol{n}^{\mathrm{f}}, \boldsymbol{n}^{\mathrm{i}}) \tag{65}$$

where $S^{\mathrm{PQ}}(\boldsymbol{n}^{\mathrm{f}}, \boldsymbol{n}^{\mathrm{i}})$ is the surface element scattering coefficient for incident waves in the direction $\boldsymbol{n}^{\mathrm{i}}$ and polarization Q = V (vertical), H (horizontal), and scattered waves in the direction $\boldsymbol{n}^{\mathrm{f}}$ and polarization P = V, H. It should be noted that the scattering coefficients $S^{\mathrm{PQ}}(\boldsymbol{n}^{\mathrm{f}}, \boldsymbol{n}^{\mathrm{i}})$ are not functions of slope. In Eq. (65), $Q(\boldsymbol{n}^{\mathrm{f}}, \boldsymbol{n}^{\mathrm{i}})$ is expressed in terms of the surface height joint characteristic function χ_2 and characteristic function χ as follows:

$$\begin{aligned} Q(\boldsymbol{n}^{\mathrm{f}}, \boldsymbol{n}^{\mathrm{i}}) = \frac{k_0^4}{\pi v_y^2} \int_{-2l}^{2l} \int_{-2L}^{2L} & \left(1 - \frac{|x_{\mathrm{d}}|}{2L}\right) \\ & \cdot \left(1 - \frac{|z_{\mathrm{d}}|}{2l}\right) (\chi_2(v_y, -v_y) \\ & - |\chi(v_y)|^2) \exp(i\boldsymbol{v} \cdot \boldsymbol{r}_{dt})\, d\boldsymbol{r}_{dt} \end{aligned} \tag{66}$$

where k_0 is the free-space wavenumber and $\boldsymbol{r}_{dt}$ is the projection of $\boldsymbol{r}_{S1} - \boldsymbol{r}_{S2}$ (where $\boldsymbol{r}_{S1}$ and $\boldsymbol{r}_{S2}$ are position vectors to two points on the rough surface) on the mean plane ($y = 0$) of the rough surface $y = h(x, z)$ (see Fig. 3):

$$\boldsymbol{r}_{dt} = x_d \boldsymbol{a}_x + z_d \boldsymbol{a}_z = \boldsymbol{r}_{S1} - \boldsymbol{r}_{S2} - (h_1 - h_2)\boldsymbol{a}_y \tag{67}$$

and $d\boldsymbol{r}_{dt} = dx_d dz_d$. The vector $\boldsymbol{v}$ is given by Eq. (44). For homogeneous isotropic surfaces with Gaussian joint surface height probability density functions

$$\chi_2 = \exp[-v_y^2 \langle h^2 \rangle (1 - R(r_d))] \tag{68}$$

$$|\chi|^2 = \exp[-v_y^2 \langle h^2 \rangle] = \chi_2(r_d \to \infty) \tag{69}$$

where v_y is the y component of $\boldsymbol{v}$ [Eq. (44)], $\langle h^2 \rangle$ is the mean-square height and $R(r_d)$ is the normalized surface height autocorrelation function [related to the Fourier transform of the surface height spectral density function $W(k)$]. When the surface is isotropic and homogeneous, R is only a function of the distance

$$r_d = \sqrt{x_d^2 + z_d^2} \tag{70}$$

and $Q(\boldsymbol{n}^f, \boldsymbol{n}^i)$ [Eq. (66)] can be expressed as follows for $L, l \gg l_c$ (the autocorrelation length):

$$Q(\boldsymbol{n}^f, \boldsymbol{n}^i) = \frac{2k_0^4}{v_y^2} \int_{-\infty}^{\infty} [\chi_2(v_y, -v_y) - |\chi(v_y)|^2] J_0(v_{xx} r_d) r_d \, dr_d \tag{71}$$

where J_0 is the Bessel function of order zero and

$$v_{xz} = (v_x^2 + v_z^2)^{1/2} = (v^2 - v_y^2)^{1/2} \tag{72}$$

Note that $Q(\boldsymbol{n}^f, \boldsymbol{n}^i)$ remains finite as $v_y \to 0$.

The above expressions based on the original full-wave solutions are in total agreement with solutions based on Rice's small perturbation solutions when the height and slopes are of the same order of smallness (3). For these cases

$$\chi_2(v_y, -v_y) - |\chi(v_y)|^2 \approx v_y^2 \langle h^2 \rangle R(r_d) \tag{73}$$

and the integrals in Eq. (66) can be expressed in closed form in terms of the rough-surface height spectral density function [the Fourier transform of the surface height autocorrelation function $\langle hh' \rangle = \langle h^2 \rangle R(r_d)$].

However, the solution [Eq. (66)] based on the original full-wave solution is not restricted to surfaces with small mean-square heights. Since it is based on the first-order single-scatter iterative solution, it is nevertheless restricted to surfaces with small slopes ($\sigma_s^2 < 0.1$).

When slopes of the rough surface are not small and the scales of roughness are very large compared to wavelength, solutions based on the transformation [Eq. (56)] can be used. Thus, the diffuse scatter cross section

is expressed as follows:

$$\sigma^{\mathrm{PQ}} = \frac{k_0^4}{\pi A_y}\int_{-l}^{l}\int_{-l}^{l}\int_{-L}^{L}\int_{-L}^{L}\frac{D_1^{\mathrm{PQ}}D_2^{\mathrm{PQ}^*}}{v_y^2}\{\exp[iv_y(h_1-h_2)] - \exp(iv_y h_1) - \exp(-iv_y h_2) + 1\}\exp[i\boldsymbol{v}\cdot(\boldsymbol{r}_{t1}-\boldsymbol{r}_{t2})]\,dx_{s1}\,dx_{s2}\,dz_{s1}\,dz_{s2} \tag{74}$$

where the symbol $*$ denotes the complex conjugate and

$$\boldsymbol{r}_{t1}-\boldsymbol{r}_{t2} = (x_{s1}-x_{s2})\boldsymbol{a}_x + (z_{s1}-z_{s2})\boldsymbol{a}_z \tag{75}$$

The (statistical) mean scattering cross section for random rough surfaces is obtained by averaging Eq. (74) over the surface heights and slopes at points r_{s1} and r_{s2}. The coherent component of Eq. (75) is defined as

$$\langle\sigma_{\mathrm{C}}^{\mathrm{PQ}}\rangle = \frac{4\pi r^2|\langle E_{\mathrm{S}}^{\mathrm{Qf}}\rangle|^2}{A_y|E^{\mathrm{Pi}}|^2} \tag{76}$$

and the incoherent scattering cross section is defined as

$$\langle\sigma_{\mathrm{I}}^{\mathrm{PQ}}\rangle \equiv \langle\sigma^{\mathrm{PQ}}\rangle - \langle\sigma_{\mathrm{C}}^{\mathrm{PQ}}\rangle \tag{77}$$

The above expression for the radar cross sections for two-dimensional random rough surfaces involves integrals over the random rough-surface heights and slopes and the surface variables x_{s1}, x_{s2}, z_{s1}, z_{s2}. This expression can be simplified significantly if the radii of curvature of the large-scale (patch) surface are assumed to be very large compared with the free-space wavelength. In this case, the slope at point 2 may be approximated by the value of the slope at point 1 ($h_{x2} \sim h_{x1}$, $h_{z2} \sim h_z 1$). If, in addition, the rough surfaces are assumed to be statistically homogeneous, the cross section is expressed as follows:

$$\langle\sigma^{\mathrm{PQ}}\rangle = \frac{k_0^4}{\pi}\int_{-2l}^{2l}\int_{-2L}^{2L}\left(1-\frac{|x_{\mathrm{d}}|}{2L}\right)\left(1-\frac{|z_{\mathrm{d}}|}{2l}\right)\left\langle\frac{f^{\mathrm{PQ}}(\boldsymbol{n}_{\mathrm{p}},\boldsymbol{n}_{\mathrm{p}})}{v_y^2}\times[\chi(v_y,-v_y|h_x,h_z)) - \chi(v_y,0|h_x,h_z) - \chi(0,-v_y|h_x,h_z)+1\right\rangle\times\exp[i(v_x x_{\mathrm{d}}+v_z z_{\mathrm{d}})]\,dx_{\mathrm{d}}\,dz_{\mathrm{d}} \tag{78}$$

in which the analytical expressions for the conditional joint characteristic functions are

$$\chi(a,b|h_x,h_z) \equiv \int_{-\infty}^{\infty}\int_{-\infty}^{\infty}\exp[i(ah_1+bh_2)]p(h_1,h_2|h_x,h_z)\,dh_1\,dh_2 \tag{79}$$

Furthermore,

$$f^{\mathrm{PQ}}(\boldsymbol{n}_{\mathrm{p}}, \boldsymbol{n}_{\mathrm{p}}) = D^{\mathrm{PQ}} D^{\mathrm{PQ}^*} U(-\boldsymbol{n}^{\mathrm{i}} \cdot \boldsymbol{n}_{\mathrm{p}}) U(\boldsymbol{n}^{\mathrm{f}} \cdot \boldsymbol{n}_{\mathrm{p}}) P_2(\boldsymbol{n}^{\mathrm{f}}, \boldsymbol{n}^{\mathrm{i}} | \boldsymbol{n}_{\mathrm{s}}) \quad (80)$$

where $P_2(\boldsymbol{n}^{\mathrm{f}}, \boldsymbol{n}^{\mathrm{i}}|\boldsymbol{n}_{\mathrm{s}})$ is Sancer's (63) shadow function and $\boldsymbol{n}_{\mathrm{s}}$ is the value of $\boldsymbol{n}_{\mathrm{p}}$ at the specular points.

For random rough surfaces characterized by a four-dimensional Gaussian surface high/slope coherence matrix we obtain

$$\chi(a, b | h_x, h_z) = \chi_2(a, b) \exp\left[\frac{-i2h_x B_x b + B_x^2 b^2}{2\sigma_x^2} + \frac{-i2h_z B_z b + B_z^2 b^2}{2\sigma_z^2}\right] \quad (81)$$

$$\chi_2(a, b) = \exp[-v_h^2 \langle h^2 \rangle (1 - C)] \quad (82)$$

$$B_x \equiv \langle h_1 h_x \rangle = -\langle h_2 h_x \rangle = -\frac{dC\langle h^2 \rangle}{dx_{\mathrm{d}}} = \sigma_x^2 x_{\mathrm{d}} C \quad (83)$$

$$B_z \equiv \langle h_1 h_{z2} \rangle = -\langle h_2 h_x \rangle = -\frac{dC\langle h^2 \rangle}{dx_{\mathrm{d}}} = \sigma_z^2 z_{\mathrm{d}} C \quad (84)$$

and

$$C(x_{\mathrm{d}}, z_{\mathrm{d}}) = \exp\left[-\left(\frac{x_{\mathrm{d}}}{l_{cx}}\right)^2 - \left(\frac{z_{\mathrm{d}}}{l_{cz}}\right)^2\right] \quad (85)$$

In Eq. (85), C is the Gaussian surface height autocorrelation function and l_{cx}, l_{cz} are correlation lengths in the x and z directions, respectively.

When the surface is isotropic ($l_{cx} = l_{cz} = l_{\mathrm{c}}$ and $\sigma^2{}_x = \sigma^2{}_z = \sigma^2{}_{\mathrm{s}}$), Eqs. (81), (83), and (84) reduce to

$$\chi(a, b | h_x, h_z) = \chi_2(a, b) \exp\left[\frac{-i2(h_x B_x + h_z B_z) b + (B_x^2 + B_z^2) b^2}{2\sigma_{\mathrm{s}}^2}\right] \quad (86)$$

where

$$B_x = \sigma_{\mathrm{s}}^2 x_{\mathrm{d}} \exp\left(-\frac{x_{\mathrm{d}}^2 + z_{\mathrm{d}}^2}{l_{\mathrm{c}}^2}\right) \quad (87)$$

and

$$B_z = \sigma_s^2 z_d \exp\left(-\frac{x_d^2 + z_d^2}{l_c^2}\right) \tag{88}$$

In this case, the total mean square slope is expressed as

$$\sigma_{sT}^2 = \frac{4\langle h^2\rangle}{l_c^2} = 2\sigma_s^2 \tag{89}$$

For the assumed isotropic surface with Gaussian statistics, the four-dimensional integral [Eq. (28) with Eqs. (86) and (88)] can be expressed as a three-dimensional integral using a Bessel function identity (4).

The resulting full-wave incoherent diffuse scatter cross section that accounts for surface height/slope correlations is expressed as

$$\begin{aligned}\langle \sigma_I^{PQ}\rangle = {} & \frac{k_0^4}{\pi v_y^2} 2\pi \iiint f^{PQ}(\boldsymbol{n},\boldsymbol{n}) \\ & \left\{ |\chi(v_y)|^2 \left[\exp\left(\frac{\sigma_s^2}{2} v_y^2 r_d^2 \exp\left(-\frac{2r_d^2}{l_c^2}\right)\right.\right. \right. \\ & \left. \left. + \langle h^2\rangle v_y^2 \exp\left(-\frac{r_d^2}{l_c^2}\right)\right) J_0(v'_{xz} r_d) - J_0(v_{xz} r_d) \right] \\ & - \chi(v_y) \left[\exp\left(\frac{\sigma_s^2}{2} v_y^2 r_d^2 \exp\left(-\frac{2r_d^2}{l_c^2}\right)\right) J_0(v'_{xz} r_d) \right. \\ & \left. \left. - J_0(v_{xz} r_d) \right] \right\} p(h_x, h_z) r_d \, dr_d \, dh_x \, dh_z \end{aligned} \tag{90}$$

where

$$\chi(v_y) = \exp\left[-\frac{v_y^2 \langle h^2\rangle}{2}\right] \tag{91}$$

Furthermore,

$$v_{xz} = \sqrt{v_x^2 + v_z^2} \tag{92}$$

and

$$v'_{xz} = \sqrt{(v'_x)^2 + (v'_z)^2} \tag{93}$$

In Eq. (93),

$$v_x' = v_x + v_y h_x \exp\left(-\frac{r_d^2}{4l_c^2}\right) \tag{94}$$

and

$$v_z' = v_z + v_y h_z \exp\left(-\frac{r_d^2}{4l_c^2}\right) \tag{95}$$

In Eq. (90), $p(h_x, h_z)$ is the probability density function for the slopes (assumed here to be Gaussian).

It is shown that the above results in which the correlations between the surface heights and slopes have been accounted for in the analysis reduce to the small perturbation results when the heights and slopes are of the same order of smallness and reduce to the physical/geometrical results in the high-frequency limit (64). These full-wave results have also been compared with numerical and experimental results for one-dimensionally (3) and two-dimensionally (64) rough surfaces.

When the rough surface consists of multiple scales of roughness as in the case of sea surfaces, two scale models have been introduced to obtain the scatter cross sections. Thus, the surface is assumed to consist of a small-scale surface that is modulated by the slopes of the large-scale surface and the cross section is expressed as a sum of the cross sections for the large- and small-scale surfaces. However, Brown (8) has shown that the hybrid-perturbation–physical-optics results critically depend upon the choice of the spatial wavenumber k_d that separates the large-scale surface from the small-scale surface. To apply this hybrid-perturbation–physical-optics approach, the Raleigh rough-surface parameter $\beta = 4k^2{}_0\langle h^2{}_s\rangle$ must be chosen to be very small compared to unity. This places a very strict restriction on the choice of k_d. As a result, scattering from the remaining surface consisting of the larger-scale spectral components with $k_l < k_d$ may not be adequately analyzed using physical optics (see Fig. 4).

The above Raleigh rough-surface parameter β does not place any restriction on the choice of k_d when the full-wave analysis is used. Furthermore, it is shown (65) that the full-wave solution for these multiple-scale rough surfaces are expressed as *weighted* sums of two cross sections:

$$\langle \sigma^{PQ} \rangle = |\chi_s|^2 \langle \sigma_l^{PQ} \rangle + \langle \sigma_s^{PQ} \rangle \tag{96}$$

where $\langle \sigma^{PQ}{}_l \rangle$ is the cross section associated with the surface consisting of the larger spectral components ($k_l < k_d$), while $\langle \sigma^{PQ}{}_s \rangle$ is the cross section associated with the surface consisting of the smaller spectral components $k_s > k_d$. Scattering by the small-scale surface is modulated by the slopes of the large-scale surface, while scattering by the small-scale surface is diminished by a coefficient (less than unity) that is equal to the magnitude of the small-scale characteristic function squared [Eq. (69)].

Thus, using the full-wave approach, extensive use is made here of the full-wave scattering cross-section modulation for arbitrarily oriented composite rough surfaces. Thus, the incoherent diffuse radar cross sections of the composite (multiple scale) rough surface is obtained by regarding the composite rough surface as an ensemble of individual patches (several correlation lengths in the lateral dimension) of arbitrary orientation (see Fig. 5). The cross section per unit area of the composite rough surface is obtained by averaging the cross sections of the individual arbitrarily oriented pixels. It is shown that the (unified full wave) cross section of the composite rough surface is relatively stationary over a broad range of patch sizes. In this broad range of values of patch sizes, the norm of the relative error is minimum.

A patch is assumed to be oriented normal to the vector (see Fig. 5)

$$\begin{aligned}\boldsymbol{a}_y &= \sin\Omega\cos\tau\boldsymbol{a}'_x + \cos\Omega\cos\tau\boldsymbol{a}'_y + \sin\tau\boldsymbol{a}'_z \\ &= (-h_x\boldsymbol{a}'_x + \boldsymbol{a}'_y - h_z\boldsymbol{a}'_x)/(1+h_x^2+h_z^2)^{1/2}\end{aligned} \tag{97}$$

where $\boldsymbol{a}'_x$, $\boldsymbol{a}'_y$, and $\boldsymbol{a}'_z$ are the unit vectors in the fixed (reference) coordinate system associated with the mean plane $y' = h_0 = 0$ and $h_x = \partial h/\partial x$, $h_z = \partial h/\partial z$. The unit vectors $\boldsymbol{a}_x$ and $\boldsymbol{a}_z$ are tangent to the mean plane of the patch. The angles Ω and τ are the tilt angles in and perpendicular to the fixed plane of incidence (the x', y' plane).

The cosines of the angles of incidence and scatter in the patch coordinate system can be expressed in terms of the cosines of the angles of incidence and scatter in the fixed reference coordinate system (primed quantities; see Fig. 5) as follows:

$$-\boldsymbol{n}^{\mathrm{i}}\cdot\boldsymbol{a}_y = \cos\theta_0^{\mathrm{i}} = \cos(\theta_0^{\mathrm{i}'} + \Omega)\cos\tau \tag{98}$$

and

$$\begin{aligned}\boldsymbol{n}^{\mathrm{f}}\cdot\boldsymbol{a}_y = \cos\theta_0^{\mathrm{f}} = &[\cos\theta_0^{\mathrm{f}'}\cos\Omega + \sin\theta_0^{\mathrm{f}'}\sin\Omega\cos\phi^{\mathrm{f}'}] \\ &\cdot\cos\tau + \sin\theta^{\mathrm{f}'}\sin\tau\end{aligned} \tag{99}$$

The surface element scattering coefficient for the tilted pixel is expressed as follows (66):

$$D_{\mathrm{p}} = T_{\mathrm{p}}^{\mathrm{f}} S_{\mathrm{p}} T_{\mathrm{p}}^{\mathrm{i}} \tag{100}$$

in which $S^{\mathrm{PQ}}{}_{\mathrm{p}}$ the elements of the 2×2 scattering matrix S_{p} are obtained from S^{PQ} on replacing the angles $\theta^{\mathrm{i}'}{}_0$ and $\theta^{\mathrm{f}'}{}_0$ by $\theta^{\mathrm{i}}{}_0$ and $\theta^{\mathrm{f}}{}_0$, respectively. Furthermore, $\cos(\phi^{\mathrm{f}\prime} - \phi^{\mathrm{i}\prime})$ and $\sin(\phi^{\mathrm{f}\prime} - \phi^{\mathrm{i}\prime})$ are replaced by the cosine and the sine of the angle $(\phi^{\mathrm{f}} - \phi^{\mathrm{i}})$ between the planes of scatter and incidence (with respect to the pixel coordinate system (see Fig. 5) (62). The matrices $T^{\mathrm{f}}{}_{\mathrm{p}}$ and $T^{\mathrm{i}}{}_{\mathrm{p}}$ relate to the vertically and horizontally polarized waves in the reference coordinate system to the vertically and horizontally polarized waves in the local (patch) coordinate system (66). Thus

$$T_{\mathrm{p}}^{\mathrm{i}} = \begin{pmatrix} \cos\psi^{\mathrm{i}} & \sin\psi^{\mathrm{i}} \\ -\sin\psi^{\mathrm{i}} & \cos\psi^{\mathrm{i}} \end{pmatrix}, \qquad T_{\mathrm{p}}^{\mathrm{f}} = \begin{pmatrix} \cos\psi^{\mathrm{f}} & -\sin\psi^{\mathrm{f}} \\ \sin\psi^{\mathrm{f}} & \cos\psi^{\mathrm{f}} \end{pmatrix} \tag{101}$$

where

$$\cos\psi^{\mathrm{i}} = \frac{\cos\tau\sin(\theta_0^{\mathrm{i}} + \Omega)}{\sin\theta_0^{\mathrm{i}}} \tag{102}$$

$$\sin\psi^{\mathrm{i}} = \frac{\sin\tau}{\sin\theta_0^{\mathrm{i}}} \tag{103}$$

$$\cos\psi^{\mathrm{f}} = [\cos\tau(\sin\theta_0^{\mathrm{f}'}\cos\Omega - \cos\theta_0^{\mathrm{f}'}\cos\phi^{\mathrm{f}'}\sin\Omega) - \cos\theta_0^{\mathrm{f}'}\sin\phi^{\mathrm{f}'}\sin\tau]/\sin\theta_0^{\mathrm{f}} \tag{104}$$

and

$$\sin\psi^{\mathrm{f}} = [\sin\tau\cos\phi^{\mathrm{f}'} - \cos\tau\sin\Omega\sin\phi^{\mathrm{f}'}]/\sin\theta_0^{\mathrm{f}} \tag{105}$$

The angles Ω and τ can be expressed in terms of the derivatives of $h(x, z)$ as follows:

$$\cos\Omega = \frac{1}{\sqrt{1+h_x^2}}, \qquad \sin\Omega = \frac{-h_x}{\sqrt{1+h_x^2}} \tag{106}$$

$$\cos\tau = \frac{\sqrt{1+h_x^2}}{\sqrt{1+h_x^2+h_z^2}}, \qquad \sin\tau = \frac{-h_z}{\sqrt{1+h_x^2+h_z^2}} \tag{107}$$

The radar cross section (per unit area) for the tilted patch can be expressed as follows:

$$\sigma_{\mathrm{p}}^{\mathrm{PQ}} = |D_{\mathrm{p}}^{\mathrm{PQ}}|^2 Q_{\mathrm{p}}(\boldsymbol{n}^{\mathrm{f}}, \boldsymbol{n}^{\mathrm{i}}) \tag{108}$$

and

$$Q_{\mathrm{p}}(\boldsymbol{n}^{\mathrm{f}}, \boldsymbol{n}^{\mathrm{i}}) = \frac{k_0^4}{\pi(\boldsymbol{a}_y'\cdot\boldsymbol{a}_y)^2 v_y^2}\int_{-2L_p}^{2L_p}\int_{-2l_{\mathrm{p}}}^{2l_{\mathrm{p}}} \cdot\left(1-\frac{|x_z|}{2L_{\mathrm{p}}}\right)\left(1-\frac{|z_{\mathrm{d}}|}{2l_{\mathrm{p}}}\right) \cdot[\chi_{2\mathrm{p}}(v_y,-v_y) - |\chi_{\mathrm{p}}(v_y)|^2]\exp(i\boldsymbol{v}\cdot\boldsymbol{r}_{\mathrm{dt}})\,d\boldsymbol{r}_{\mathrm{dt}} \tag{109}$$

where

$$\boldsymbol{a}_y'\cdot\boldsymbol{a}_y = [1+h_x^2+h_z^2]^{-1/2} \tag{110}$$

$$\boldsymbol{v} = \boldsymbol{k}_0^{\mathrm{f}} - \boldsymbol{k}_0^{\mathrm{i}} = v_x'\boldsymbol{a}_x' + v_y'\boldsymbol{a}_y' + v_z'\boldsymbol{a}_z' \tag{111}$$

in which

$$v_y = \boldsymbol{v}\cdot\boldsymbol{a}_y = v_x'\sin\Omega\cos\tau + v_y'\cos\Omega\cos\tau + v_z'\sin\tau, v_{\mathrm{t}} = (v^2 - v_y^2)^{1/2} \tag{112}$$

Thus, in Eq. (108) both $|D^{\mathrm{PQ}}{}_{\mathrm{p}}|^2$ and Q_{p} are functions of the slopes h_x and h_z of the tilted patch mean plane (see Fig. 5). For a deterministic composite rough surface, the slopes (that modulate the orientation of the

patch) are known. The radar scatter cross section for this composite surface is given by summing the fields of the individual patches. However, if the composite surface height is random, the tilted pixel cross section (per unit area) [Eq. (108)] for the rough surface is also a random function of the pixel orientation. Thus, in order to determine the cross section per unit area of the composite random rough surface, it is necessary to evaluate the statistical average of $\sigma^{PQ}{}_p$. The cross section of the composite random rough surface is given by

$$\langle \sigma_p^{PQ} \rangle = \langle |D_p^{PQ}|^2 Q_p(\boldsymbol{n}^f, \boldsymbol{n}^i) \rangle \tag{113}$$

where $\langle \cdot \rangle$ denotes the statistical average (over the slope probability density function $p(h_x, h_z)$ of the tilted patch). The mean-square slope of the tilted patch is given in terms of the surface height spectral density function

$$\sigma_p^2 = 2\pi \int_0^{k_p} \frac{W(k)}{4} k^3 \, dk \tag{114}$$

For the case $k_p \to 0, L_p, l_p \to \infty, \sigma_p \to 0$, the cross section $\langle \sigma^{PQ}{}_p \rangle$ reduces to the original full-wave solution $\langle \sigma^{PQ}{}_0 \rangle$ [Eq. (65)]. In Eq. (114), the upper limit k_p is the wavenumber associated with the patch of lateral dimension $L_p = 2\pi/k_p$.

In the expression for $Q_p(\boldsymbol{n}^f, \boldsymbol{n}^i)$ [Eq. (109)], the surface height autocorrelation function for the rough surface associated with the patch is given in terms of the Fourier transform of the surface height spectral density function as follows:

$$\begin{aligned} \langle h_{p1} h_{p2} \rangle &= \langle h_p^2 \rangle R_s(r_d) = \langle h^2 \rangle R(r_d) \\ &\quad - \iint_{-k_p}^{k_p} \frac{W(k_x, k_z)}{4} \\ &\quad \cdot \exp[ik_x x_d + ik_z z_d] dk_x \, dk_z \\ &= 2\pi \int_{k_p}^{\infty} \frac{W(k)}{4} J_0(kr_d) k \, dk \end{aligned} \tag{115}$$

where it is assumed that the surface is homogeneous and isotropic, $k = (k^2{}_x + k^2{}_z)^{1/2}$.

Illustrative examples of the results obtained for the scatter cross section using the above procedures have been published (66).

For purposes of comparisons, the generalized telegraphists' equations [Eqs. (32) and (33)] have also been solved numerically for one-dimensionally rough surfaces (67). The procedures used are outlined here. On extending the range of the wave vector variable u from $-\infty$ to ∞, the Eqs. (32) and (33) are combined into one coupled integrodifferential equation for the forward and backward scattered wave amplitudes $a(x, u)$ and $a(x, -u)$, respectively.

On extracting the rapidly changing part $\exp(-iux)$, the wave amplitudes are expressed as

$$a^P(x, u) = A^P(x, u) \exp(-iux) \tag{116}$$

The total wave amplitude is the sum of the source-dependent primary wave amplitude $A^P{}_p$ and the diffusely scattered wave amplitude $A^P{}_s$ due to the surface roughness:

$$A^P(x, u) = A_p^P(x, u) + A_s^P(x, u) \tag{117}$$

The primary wave amplitude is obtained from Eqs. (32) and (33) on ignoring the coupling terms $S^{\alpha\beta}{}_{PQ}$. The resulting integrodifferential equation for the diffusely scattered term $A^{P}{}_{s}$ is converted into an integral equation with mixed boundary conditions. This expression is integrated by parts to get rid of the singularity in the scattering coefficient. The resulting integral equation is solved numerically using the standard moments method. Finally the field transforms [Eqs. (17) and (18)] are used to obtain the results for the electromagnetic fields from the wave amplitudes. For the far fields, these expressions can be integrated analytically (over the wavenumber variable) using stationary-phase techniques. These results show that for surfaces with small to moderate slopes the proceeding analytical results are valid (67).

When the observation points are near the surface, it is necessary to account for coupling between the radiation fields, the lateral waves, and the surface waves associated with rough surface scattering (68,69). When the rough surface is assumed to be perfectly conducting, the contribution from the branch cut integral associated with the lateral waves vanishes and there are no residue contributions (associated with surface waves) from the singularities of the reflection coefficients. When the approximate impedance boundary condition is used, the lateral wave contribution is eliminated.

The full-wave method can also be used to determine the fields scattered upon transmission across rough surfaces (70). When scattering from more than one rough interface in an irregular stratified media is considered, in general, it becomes necessary to account for scattering upon reflection and transmission across rough surfaces. This topic is reviewed in the next section.

Full-Wave Solutions for Three Media Irregular Stratified Structures

Full-wave solutions are derived for the electromagnetic fields scattered by the two rough surfaces in a realistic physical model of a three media environment. They account for five different scattering mechanisms that the waves undergo, assuming that both the transmitter and receiver are above the uppermost interface of the irregular media. Two scattering mechanisms are associated with reflection from above and below the upper interface, and two are associated with transmission across the upper interface; the fifth is associated with reflection from above the lower interface.

In view of the fact that in general the two rough interfaces are characterized by independent random rough surface heights (except where the thickness of the intermediate medium vanishes) the rough surface height joint probability density functions are characterized by a family of probability density functions associated with the gamma functions. Multiple bounces between the two interfaces are accounted for in the analysis. The elements of the incoherent Mueller matrix (that relates the scattered to the incident Stokes vectors) can be obtained from the expressions for the scattered fields. From the simulated data it is possible, for instance, to determine the optimal polarizations and the incident and scatter angles of the waves as well as the wavelength, for purposes of suppressing or enhancing the impact of the clutter from the rough interfaces. This work can be used to provide realistic models of electromagnetic scattering from snow-covered terrain, ice-covered sea surfaces, naturally occurring or man-made oil slicks, and coated rough surfaces. The models can be used to reduce the impact of signal clutter from the rough interfaces, to facilitate the detection of buried objects.

The diffusely scattered electromagnetic fields for the two irregular structures illustrated in Fig. 6 were investigated initially. In model 1, the upper interface is flat and the lower interface is rough (71,72,73,74). In model 2, the upper interface is rough and the lower interface is flat (75).

In this work, the model of the irregular structure considered consists of two random rough (upper and lower) interfaces. The thickness of the coating material (film) between the two random rough interfaces is assumed to be arbitrary. The physical mechanism for scattering from coated rough surfaces is schematically

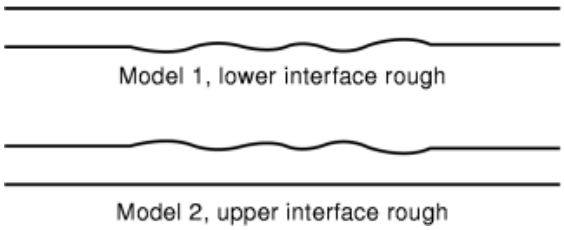

Fig. 6. Two previously investigated models with only one rough interface.

illustrated in Fig. 7. The upper interface for $y = h_{01s}(x_s, z_s)$ between medium 0 and medium 1 is

$$h_{01s}(x_s, z_s) = \begin{cases} h_{s1}(x_s, z_s), & |x_s| < l, |z_s| < L \\ h_{01}, & |x_s| \geq l, |z_s| \geq L \end{cases} \tag{118}$$

where the mean value of h_{01s} is $< h_{01s} >= h_{01}$. The lower interface $y = h_{12s}(x_s, z_s)$ between medium 1 and medium 2 is

$$h_{12s}(x_s, z_s) = \begin{cases} h_{s1}(x_s, z_s), & |x_s| \leq l, |z_s| \leq L \\ h_{12}, & |x_s| > l, |z_s| > L \end{cases} \tag{119}$$

The thickness of the coating layer, H_D, is

$$H_D(x_s, z_s) = h_{01s}(x_s, z_s) - h_{12s}(x_s, z_s) \tag{120}$$

The unit vectors normal to the large-scale rough interfaces between medium 0 and 1 and between medium 1 and 2 are

$$\boldsymbol{n} = \frac{-h_x \boldsymbol{a}_x + \boldsymbol{a}_y - h_x \boldsymbol{a}_z}{\sqrt{1 + h_x^2 + h_z^2}} = \sin\gamma \cos\delta \boldsymbol{a}_x + \cos\delta \boldsymbol{a}_y + \sin\gamma \sin\delta \boldsymbol{a}_z \tag{121}$$

where

$$h_x = \frac{dh_{s1,2}}{dx_s}, \qquad h_z = \frac{dh_{s1,2}}{dz_s} \tag{122}$$

$$\gamma = \arccos\left[\frac{1}{\sqrt{1 + h_x^2 + h_z^2}}\right], \qquad \delta = \arctan\left[\frac{h_x}{h_z}\right] \tag{123}$$

Using the full-wave approach (71), the diffuse first-order scattered fields can be expressed as the sum

$$E_S^{PQ} = E_{SU}^{PQ}(\boldsymbol{r}) + E_{SD}^{PQ}(\boldsymbol{r}) \tag{124}$$

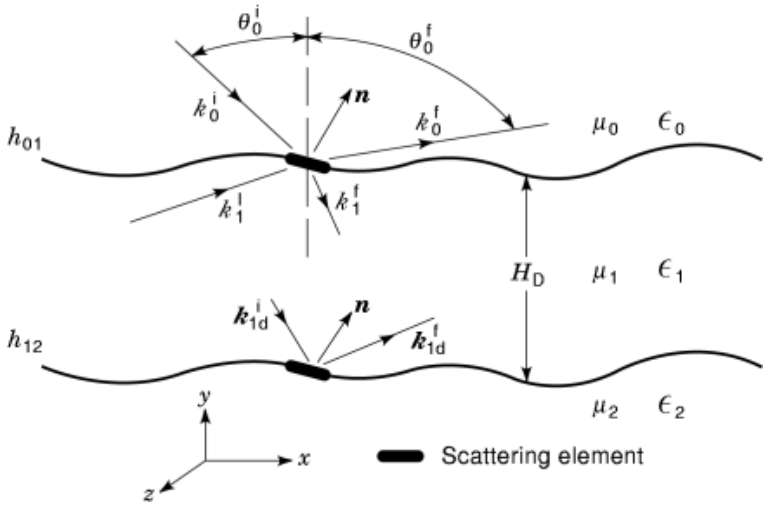

Fig. 7. Irregular layered model with two rough interfaces.

where $E^{PQ}{}_{SU}(\boldsymbol{r})$ is associated with scattering from the upper interface, and $E^{PQ}{}_{SD}(\boldsymbol{r})$ is associated with scattering from the lower interface. For e^{iwt} time harmonic plane wave excitations, the incident electric field of magnitude $E^{iP}{}_0$ is

$$\boldsymbol{E}_P^i = E_0^{iP} e^{-ik_0^i \cdot \boldsymbol{r}} \boldsymbol{a}_P \tag{125}$$

In Eq. (125), $\boldsymbol{a}_P$ is parallel (P = V) or perpendicular (P = H) to the reference plane of incidence (normal to $\boldsymbol{n}^i{}_0 \times \boldsymbol{a}_y$ where $\boldsymbol{n}^i{}_0$ is the unit vector in the direction of the wave vector $\boldsymbol{k}^i{}_0$ for the incident waves). For plane-wave excitations and for observation points above the upper interface $y \geq h_{01s}(x_s, z_s)$ the scattered fields due to the rough upper and lower interfaces are given by (72,75,76,77).

$$\begin{aligned} E_{SU}^{PQ}(\boldsymbol{r}) = \frac{E_0^{Qi}}{(2\pi i)^2} \iiint \frac{e^{i(\boldsymbol{k}_0 - \boldsymbol{k}_0^i)\cdot \boldsymbol{r}_{s1} - i\boldsymbol{k}_0 \cdot \boldsymbol{r}}}{s_0^i c_\phi^i - s_0 c_\phi} \Bigg\{ & F_{00U}^{PQ}(\boldsymbol{k}, \boldsymbol{k}_0^i) \\ & + \frac{T_{01}^{Qi} R_{21}^{Qi} F_{01U}^{PQ}(\boldsymbol{k}, \boldsymbol{k}_0^i) e^{-i2v_1^i H_D}}{1 - R_{01}^{Qi} R_{21}^{Qi} e^{-i2v_1^i H_D}} \\ & + \frac{\frac{c_0}{c_1} F_{10U}^{PQ}(\boldsymbol{k}, \boldsymbol{k}_1^i) R_{21}^P T_{01}^P e^{-i2v_1^i H_D}}{1 - R_{01}^P R_{21}^P e^{-i2v_1^i H_D}} \\ & - \frac{n_r \frac{c_0}{c_1} T_{10}^{Qi} R_{21}^{Qi} \cdot F_{11U}^{PQ}(\boldsymbol{k}, \boldsymbol{k}_1^i) R_{21}^P T_{01}^P e^{-i2v_1^i H_D - i2v_1 H_D}}{[1 - R_{01}^{Qi} R_{21}^{Qi} e^{-i2v_1^i H_D}][1 - R_{01}^P R_{21}^P e^{-i2v_1^i H_D}]} \Bigg\} \\ & \frac{dh_{s1}}{dx_s} dx_s dz_s \frac{k_0}{u} dv_0 dw \end{aligned} \tag{126}$$

$$E_{\mathrm{SD}}^{\mathrm{PQ}}(\boldsymbol{r}) = \frac{E_0^{\mathrm{Qi}}}{(2\pi)^2} \iiint \frac{e^{i(\boldsymbol{k}_0 - \boldsymbol{k}_{1\mathrm{D}}^{\mathrm{i}})\cdot \boldsymbol{r}_{\mathrm{s}2} - i\boldsymbol{k}_0 \cdot \boldsymbol{r}} F_{11\mathrm{U}}^{\mathrm{PQ}}(\boldsymbol{k}, \boldsymbol{k}_{1\mathrm{D}}^{\mathrm{i}}) T_{10}^{\mathrm{Qi}} T_{10}^{\mathrm{P}}}{(s_1^{\mathrm{i}} c_\phi^{\mathrm{i}} - s_1 c_\phi)[1 - R_{01}^{\mathrm{Qi}} R_{21}^{\mathrm{Qi}} e^{-i2v_1^{\mathrm{i}} H_{\mathrm{D}}}][1 - R_{01}^{\mathrm{P}} R_{21}^{\mathrm{P}} e^{-i2v_1^{\mathrm{i}} H_{\mathrm{D}}}]} \times N^{\mathrm{PQ}} \frac{dh_{\mathrm{s}2}}{dx_{\mathrm{s}}} dx_{\mathrm{s}} dz_{\mathrm{s}} \frac{K_0}{u} dv_0 \, dw \tag{127}$$

where $F^{\mathrm{PQ}}{}_{mn\mathrm{U}}(m, n = 0, 1)$ and $F^{\mathrm{PQ}}{}_{11\mathrm{D}}$ are scattering coefficients associated with the upper and lower interfaces. The integration is over the rough surface variables x_{s} and z_{s} as well as the wave number variables v_0 and w of the scattered wave vector $\boldsymbol{k}_0$. The superscripts of $E^{\mathrm{PQ}}{}_{\mathrm{s}}$ denote P (P = H, V) polarized scattered fields due to Q (Q = H, V) polarized incident fields. The fields expressed by Eqs. (126) and (127) are at the observation point $y \geq h_{01\mathrm{s}}$:

$$\boldsymbol{r} = x\boldsymbol{a}_x + y\boldsymbol{a}_y + z\boldsymbol{a}_z \tag{128}$$

The position vectors to points on the upper and lower rough interfaces are

$$\boldsymbol{r}_{\mathrm{s}1} = x_{\mathrm{s}}\boldsymbol{a}_x + h_{\mathrm{s}1}(x_{\mathrm{s}}, z_{\mathrm{s}})\boldsymbol{a}_y + z_{\mathrm{s}}\boldsymbol{a}_z \tag{129}$$

$$\boldsymbol{r}_{\mathrm{s}2} = x_{\mathrm{s}}\boldsymbol{a}_x + h_{\mathrm{s}2}(x_{\mathrm{s}}, z_{\mathrm{s}})\boldsymbol{a}_y + z_{\mathrm{s}}\boldsymbol{a}_z \tag{130}$$

The incident and scattered wave vectors are

$$\begin{aligned} \boldsymbol{k}_j^{\mathrm{i}} &= k_j \boldsymbol{n}_j^{\mathrm{i}} = k_j[\sin\theta_{\mathrm{j}}^{\mathrm{i}} \cos\phi^{\mathrm{i}} \boldsymbol{a}_x \mp \cos\theta_{\mathrm{j}}^{\mathrm{i}} \boldsymbol{a}_y + \sin\theta_{\mathrm{j}}^{\mathrm{i}} \sin\phi^{\mathrm{i}} \boldsymbol{a}_z] \\ &= k_j[s_j^{\mathrm{i}} c_\phi^{\mathrm{i}} \boldsymbol{a}_x \mp c_j^{\mathrm{i}} \boldsymbol{a}_y + s_j^{\mathrm{i}} s_\phi^{\mathrm{i}} \boldsymbol{a}_z], \qquad \text{for} \quad j = 0, 1 \end{aligned} \tag{131}$$

$$\boldsymbol{k}_j = k_j \boldsymbol{n}_j = k_j[s_j c_\phi \boldsymbol{a}_x + c_j \boldsymbol{a}_y + s_j s_\phi \boldsymbol{a}_z], \qquad j = 0, 1, 2 \tag{132}$$

$$\begin{aligned} \boldsymbol{k}_{1\mathrm{D}}^{\mathrm{i}} = k_1 \boldsymbol{n}_{1\mathrm{D}}^{\mathrm{i}} &= k_1[\sin\theta_1^{\mathrm{i}} \cos\phi^{\mathrm{i}} \boldsymbol{a}_x - \cos\theta_1^{\mathrm{i}} \boldsymbol{a}_y + \sin\theta_1^{\mathrm{i}} \sin\phi^{\mathrm{i}} \boldsymbol{a}_z] \\ &= k_1[s_1^{\mathrm{i}} c_\phi^{\mathrm{i}} \boldsymbol{a}_x - c_1^i \boldsymbol{a}_y + s_1^{\mathrm{i}} s_\phi^{\mathrm{i}} \boldsymbol{a}_z] \end{aligned} \tag{133}$$

$$\boldsymbol{k}_{1\mathrm{D}} = k_1 \boldsymbol{n}_{1\mathrm{D}} = k_1[s_1 c_\phi \boldsymbol{a}_x + c_1 \boldsymbol{a}_y + s_1 s_\phi \boldsymbol{a}_z] \tag{134}$$

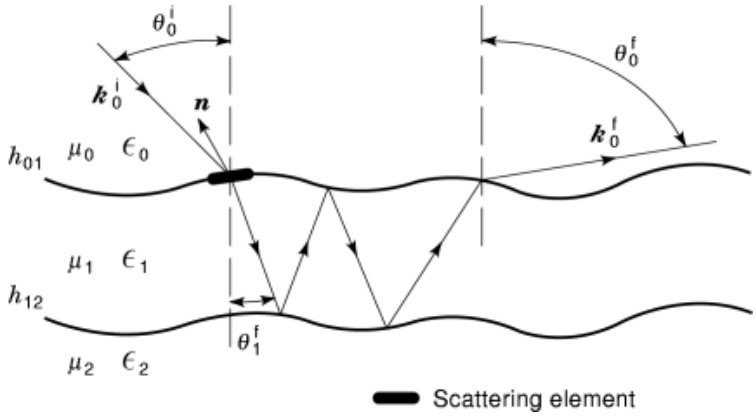

Fig. 8. Scattering upon reflections in medium 0 above the upper interface.

In Eqs. (131)–(134) the complex sines and cosines of the incident and scatter angles in medium 1 and 2 are related by Snell's law:

$$k_0 s_0 = k_1 s_1 = k_2 s_2: \qquad c_j = \sqrt{1 - s_j^2}, \quad \mathrm{Im}[k_j c_j] \le 0 \qquad j = 0, 1, 2 \tag{135}$$

Equations (126) and (127) contain the expressions for the Fresnel reflection ($R^{\mathrm{P}}{}_{\alpha\beta}$) and transmission ($T^{\mathrm{P}}{}_{\alpha\beta}$) coefficients for vertically and horizontally polarized waves, the wave impedance η, and refractive index n (76).

The physical interpretations of Eqs. (126) and (127) are illustrated in Figs. 8 to 12 (71,72,75,76). Equation (126) represents scattering due to the upper rough interface, and Eq. (127) represents scattering due to the lower rough interface. The first term on the right-hand side of Eq. (126) associated with the scattering coefficient $F^{\mathrm{PQ}}{}_{00\mathrm{U}}$ accounts for scattering upon reflection from above the rough upper interface (see Fig. 8). The second term in Eq. (126) associated with $F^{\mathrm{PQ}}{}_{01\mathrm{U}}$ accounts for waves that undergo multiple reflections in medium 1 and are scattered upon transmission back to 0 (see Fig. 9). The third term in Eq. (126) associated with $F^{\mathrm{PQ}}{}_{10\mathrm{U}}$ accounts for scattering upon transmission from medium 0 to 1 followed by multiple reflections in medium 1 before wave transmission back to medium 0 (see in Fig. 10). The fourth term in Eq. (126) associated with $F^{\mathrm{PQ}}{}_{11\mathrm{U}}$ accounts for multiple reflections in medium 1 before scattering upon reflection in medium 1 from below the upper interface, followed by multiple reflections in medium 1 before transmission back to medium 0 (see Fig. 11). The single term in Eq. (127) associated with the scattering coefficient $F^{\mathrm{PQ}}{}_{11\mathrm{D}}$ accounts for multiple reflections in medium 1 before scattering upon reflection in medium 1 from above the lower interface, followed by multiple reflections in medium 1 before transmission back to medium 0 (see Fig. 12). It is shown that for uniform layered structures, the full-wave solutions sum up to the classical solutions (71,72,73,74,75).

The diffuse scattered fields are evaluated at a point in the far-field region above the upper interface. The stationary phase method is used to evaluate the integrals over the scatter wave vector variables v_0 and w in Eqs. (126) and (127). Thus, the scattered far fields at $\boldsymbol{r}^{\mathrm{f}}$ (the position vector from origin to the receiver) are

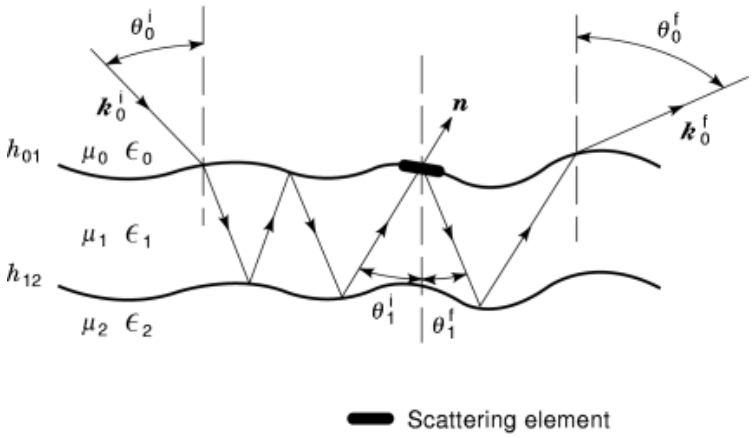

Fig. 9. Scattering upon transmission (across upper interface) from medium 1 to medium 0.

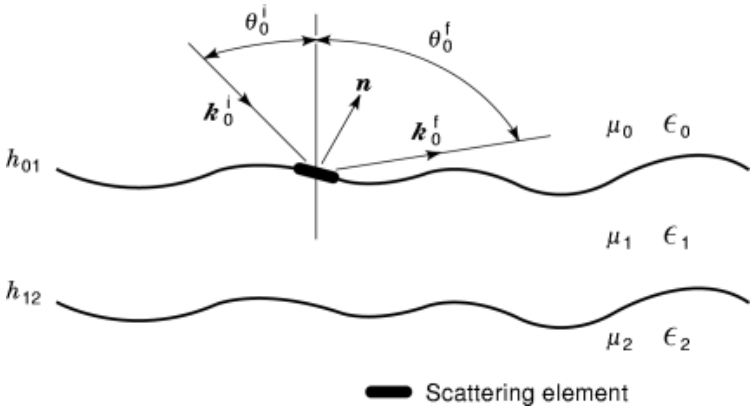

Fig. 10. Scattering upon transmission (across upper interface) from medium 0 to medium 1.

expressed as follows:

$$
\begin{aligned}
&E_{\mathrm{SU}}^{\mathrm{PU}}(\boldsymbol{r}) \\
&\quad = E^{\mathrm{Qi}} G_0 \int_{-L}^{L}\int_{-l}^{l} \frac{e^{i(\boldsymbol{k}_0-\boldsymbol{k}_0^{\mathrm{i}})\cdot \boldsymbol{r}_{s1}} - e^{i(\boldsymbol{k}_0-\boldsymbol{k}_0^{\mathrm{i}})\cdot \boldsymbol{r}_{s10}}}{c_0^{\mathrm{f}} + c_0^{\mathrm{i}}} \Bigg[F_{00\mathrm{U}}^{\mathrm{PQ}}(\boldsymbol{k}_0^{\mathrm{f}}, \boldsymbol{k}_0^{\mathrm{i}}) \\
&\qquad + T_{10}^{\mathrm{Qi}} R_{21}^{\mathrm{Qi}} F_{01\mathrm{U}}^{\mathrm{PQ}}(\boldsymbol{k}_0^{\mathrm{f}}, \boldsymbol{k}_1^{\mathrm{i}}) R^{\mathrm{Qi}} e^{-i2v_1^{\mathrm{i}} H_{\mathrm{D}}} \\
&\qquad + \frac{c_0^{\mathrm{f}}}{c_1^{\mathrm{f}}} F_{10\mathrm{U}}^{\mathrm{PQ}}(\boldsymbol{k}_1^{\mathrm{f}}, \boldsymbol{k}_0^{\mathrm{i}}) R_{21}^{\mathrm{Pf}} T_{01}^{\mathrm{Pf}} R^{\mathrm{Pf}} e^{-i2v_1^{\mathrm{f}} H_{\mathrm{D}}} \\
&\qquad - n_{\mathrm{r}} \frac{c_0^{\mathrm{f}}}{c_1^{\mathrm{f}}} T_{10}^{\mathrm{Qi}} R_{21}^{\mathrm{Qi}} F_{11\mathrm{U}}^{\mathrm{PQ}}(\boldsymbol{k}_1^{\mathrm{f}}, \boldsymbol{k}_1^{\mathrm{i}}) R_{21}^{\mathrm{Pf}} T_{01}^{\mathrm{Pf}} R^{\mathrm{Qi}} R^{\mathrm{Pf}} e^{i2(v_1^{\mathrm{i}}+v_1^{\mathrm{f}})H_{\mathrm{D}}} \Bigg] \\
&\qquad dx_s\, dz_s \\
&\quad = S_{\mathrm{U}}^{\mathrm{PU}} E_0^{\mathrm{Qi}} G_0
\end{aligned}
\tag{136}
$$

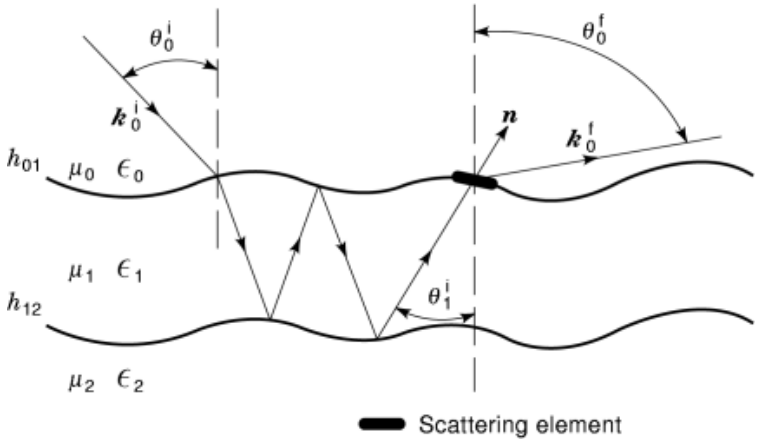

Fig. 11. Scattering upon reflection (in medium 1) below the upper interface.

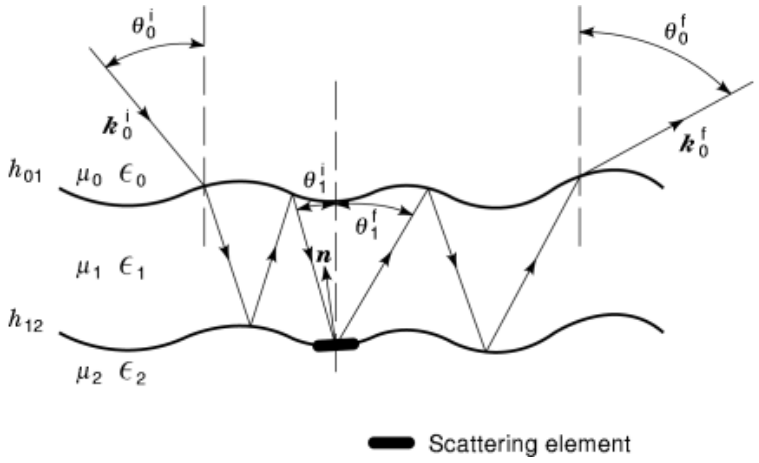

Fig. 12. Scattering upon reflection (in medium 1) above the lower interface.

and

$$E_{\mathrm{SD}}^{\mathrm{PQ}}(\boldsymbol{r}) = E_0^{\mathrm{Qi}} G_0 \int_{-L}^{L}\int_{-l}^{l} \frac{e^{i(\boldsymbol{k}_{1\mathrm{D}}^{\mathrm{f}}-\boldsymbol{k}_{1\mathrm{D}}^{\mathrm{i}})\cdot \boldsymbol{r}_{s2}} - e^{i(\boldsymbol{k}_{1\mathrm{D}}^{\mathrm{f}}-\boldsymbol{k}_{1\mathrm{D}}^{\mathrm{i}})\cdot \boldsymbol{r}_{s20}}}{c_1 + c_1^{\mathrm{i}}} F_{11\mathrm{D}}^{\mathrm{PQ}}(\boldsymbol{k}_1^{\mathrm{f}}, \boldsymbol{k}_1^{\mathrm{i}}) T_{10}^{\mathrm{Qi}} T_{01}^{\mathrm{f}} N^{\mathrm{PQ}} R^{\mathrm{Qi}} R^{\mathrm{Pf}}\, dx_s\, dz_s$$
$$= S_{\mathrm{D}}^{\mathrm{PQ}} E_0^{\mathrm{Qi}} G_0 \tag{137}$$

where the position vectors to the mean upper and lower surfaces are

$$\boldsymbol{r}_{s10} = x_s \boldsymbol{a}_x + h_{01}\boldsymbol{a}_y + z_s \boldsymbol{a}_z \tag{138}$$

$$\boldsymbol{r}_{s20} = x_s \boldsymbol{a}_x + h_{12} \boldsymbol{a}_y + z_s \boldsymbol{a}_z \tag{139}$$

and

$$G_0 = -\frac{ik_0}{2\pi r^{\mathrm{f}}} e^{-ik_0 r^{\mathrm{f}}} \tag{140}$$

The wave vectors associated with scattering in the media are

$$\begin{aligned} \boldsymbol{k}_j^{\mathrm{f}} &= k_j \boldsymbol{n}^{\mathrm{f}} = k_j[\sin\theta_j^{\mathrm{f}} \cos\phi^{\mathrm{f}} \boldsymbol{a}_x \pm \cos\theta_j^{\mathrm{f}} \boldsymbol{a}_y + \sin\theta_j^{\mathrm{f}} \sin\phi^{\mathrm{f}} \boldsymbol{a}_z] \\ &= k_j[s_j^{\mathrm{f}} c_\phi^{\mathrm{f}} \boldsymbol{a}_x \pm c_j^{\mathrm{f}} \boldsymbol{a}_y + s_j^{\mathrm{f}} s_\phi^{\mathrm{f}} \boldsymbol{a}_z] \qquad \text{for } j = 0, 1 \end{aligned} \tag{141}$$

$$\begin{aligned} \boldsymbol{k}_{1\mathrm{D}}^{\mathrm{f}} &= k_1 \boldsymbol{n}_{1\mathrm{D}}^{\mathrm{f}} = k_1[\sin\theta_1^{\mathrm{f}} \cos\phi^{\mathrm{f}} \boldsymbol{a}_x + \cos\theta_1^{\mathrm{f}} \boldsymbol{a}_y + \sin\theta_1^{\mathrm{f}} \sin\phi^{\mathrm{f}} \boldsymbol{a}_z] \\ &= k_1[s_1^{\mathrm{f}} c_\phi^{\mathrm{f}} \boldsymbol{a}_x + c_j^{\mathrm{f}} \boldsymbol{a}_y + s_j^{\mathrm{f}} s_\phi^{\mathrm{f}} \boldsymbol{a}_z] \end{aligned} \tag{142}$$

and the terms associated with multiple bounces in the coating material are

$$\begin{aligned} R^{\mathrm{Qi}} &= [1 - R_{01}^{\mathrm{Qi}} R_{21}^{\mathrm{Qi}} e^{-i2v_1^{\mathrm{i}} H_{\mathrm{D}}}]^{-1} \\ &= 1 + \cdots (R_{01}^{\mathrm{Qi}} R_{21}^{\mathrm{Qi}} e^{-iv_y^{\mathrm{i}} H_{\mathrm{D}}})^{\mathrm{q}} + \cdots, \qquad q = 1, 2, 3 \ldots \end{aligned} \tag{143}$$

$$\begin{aligned} R^{\mathrm{Pf}} &= [1 - R_{01}^{\mathrm{Pf}} R_{21}^{\mathrm{Pf}} e^{-i2v_1^{\mathrm{i}} H_{\mathrm{D}}}]^{-1} \\ &= 1 + \cdots (R_{01}^{\mathrm{Pf}} R_{21}^{\mathrm{Pfi}} e^{-iv_y^{\mathrm{i}} H_{\mathrm{D}}})^{\mathrm{p}} + \cdots, \qquad p = 1, 2, 3 \ldots \end{aligned} \tag{144}$$

The geometric series expansions appearing in Eqs. (142) and (143) are used whenever $H_{\mathrm{D}}(x_{\mathrm{s}}, z_{\mathrm{s}})$ is not constant, in order to perform necessary integrations by parts that explicitly involve the derivative of the rough surface heights (75).

The normalization coefficients are

$$N^{\mathrm{PQ}} = \begin{cases} \eta_{\mathrm{r}1} \\ 1 \\ \dfrac{1}{\eta_{\mathrm{r}i}} \end{cases} \quad \text{where } \eta_i = \sqrt{\frac{\eta_i}{\epsilon_i}} (i = 0, 1, 2), \eta_{\mathrm{r}0} = \frac{\eta_1}{\eta_0}, \eta_{\mathrm{r}1} = \frac{\eta_2}{\eta_1} \tag{145}$$

For parallel stratified structures (no roughness), the full-wave solutions reduce to the exact, classical solution. The solutions for the like- and cross-polarized diffuse scattered fields presented here can be applied to scattering from irregular layered media with arbitrarily varying rough interfaces such that the thickness of

the intermediate layer is also arbitrary when random rough surfaces are considered. The rough surface height probability density functions are characterized by a family of gamma functions rather than the standard Gaussian probability density functions to ensure that $H_D(x_s, z_s) \geq 0$ (78).

The polarimetric solutions can be applied to remote sensing of dielectric coating materials on rough surfaces. In particular, it is possible to determine the optimal polarizations of the transmitter and receiver such that the presence of clutter from the rough interfaces can be suppressed, in order to facilitate the detection of buried mines for example.

Acknowledgments

The manuscript was prepared by Ronda Vietz and Dr. Dana Poulain in the Center for Electro-Optics.

BIBLIOGRAPHY

1. S. O. Rice, Reflection of electromagnetic waves from a slightly rough surface, *Commun. Pure Appl. Math.*, **4**: 351–378, 1951.
2. G. R. Valenzuela, Scattering of electromagnetic waves from a tilted slightly rough surface, *Radio Sci.*, **3** (11): 1051–1066, 1968.
3. E. Bahar, B. S. Lee, Full wave solutions for rough surface bistatic radar cross sections: Comparison with small perturbation, physical optics, numerical, and experimental results, *Radio Sci.*, **29** (2): 407–429, 1994.
4. P. Beckmann, A. Spizzichino, *The Scattering of Electromagnetic Waves from Rough Surfaces*, New York: Macmillan, 1963.
5. D. E. Barrick, W. H. Peake, A review of scattering from surfaces with different roughness scales, *Radio Sci.*, **3** (8): 865–868, 1968.
6. J. T. Johnson *et al.*, Backscatter enhancement of electromagnetic waves from two dimensional perfectly conducting random rough surfaces: A comparison of Monte Carlo simulations with experimental data, *IEEE Trans. Antennas Propag.*, **44** (5): 748–756, 1996.
7. J. W. Wright, A new model for sea clutter, *IEEE Trans. Antennas Propag.*, **AP-16** (2): 217–223, 1968.
8. G. S. Brown, Backscattering from a Gaussian-distributed perfectly conducting rough surface, *IEEE Trans. Antennas Propag.*, **AP-28**: 943–946, 1978.
9. G. L. Tyler, Wavelength dependence in radio wave scattering and specular-point theory, *Radio Sci.*, **11** (2): 83–91, 1976.
10. E. R. Mendez, K. A. O'Donnell, Observation of depolarization and backscattering enhancement in light scattering from Gaussian random surfaces, *Opt. Commun.*, **61** (2): 91–95, 1987.
11. A. A. Maradudin, E. R. Mendoz, Enhanced backscatter of light from weakly rough random metal surfaces, *Appl. Opt.*, **32** (19): 3335–3343, 1993.
12. E. Bahar, M. El-Shenawee, Vertically and horizontally polarized diffuse multiple scatter cross sections of one dimensional random rough surfaces that exhibit enhanced backscatter-full wave solutions, *J. Opt. Soc. Amer. A*, **11** (8): 2271–2285, 1994.
13. E. Bahar, M. El-Shenawee, Enhanced backscatter from one-dimensional random rough surfaces: Stationary-phase approximations to full wave solutions, *J. Opt. Soc. Amer.*, **12** (1): 151–161, 1995.
14. J. C. Daley, W. T. Davis, N. R. Mills, Radar sea return in high sea states, *Nav. Res. Lab. Rep.*, **7142**: 1970.
15. E. Bahar, M. A. Fitzwater, Like and cross polarized scattering cross sections for random rough surfaces—Theory and experiment, *J. Opt. Soc. Amer., Spec. Issue Wave Propag. Scattering Random Media*, **2** (12): 2295–2303, 1985.
16. E. Bahar, Depolarization of electromagnetic waves excited by distribution of electric and magnetic sources in inhomogeneous multilayered structures of arbitrarily varying thickness—Generalized field transforms, *J. Math. Phys.*, **14** (11): 1502–1509, 1973.
17. E. Bahar, Depolarization of electromagnetic waves excited by distribution of electric and magnetic sources in inhomogeneous multilayered structures of arbitrarily varying thickness—Full wave solutions, *J. Math. Phys.*, **14** (11): 1510–1515, 1973.
18. E. Bahar, Depolarization in nonuniform multilayered structures—Full wave solutions, *J. Math. Phys.*, **15** (2): 202–208, 1974.

19. S. A. Schelkunoff, Generalized telegraphists' equations for waveguides, *Bell Syst. Tech. J.*, **31**: 784–801, 1952.
20. S. A. Schelkunoff, Conversion of Maxwell's equations into generalized telegraphists' equations, *Bell Syst. Tech. J.*, **34**: 995–1045, 1955.
21. E. Bahar, Propagation of radio waves in a model nonuniform terrestrial waveguide, *Proc. Inst. Electr. Eng.*, **113** (11): 1741–1750, 1966.
22. E. Bahar, Generalized scattering matrix equations for waveguide structures of varying surface impedance boundaries, *Radio Sci.*, **2** (3): 287–297, 1967.
23. E. Bahar, Wave propagation in nonuniform waveguides with large flare angles and near cutoff, *IEEE Trans. Microw.Theory Tech.*, **MTT-16** (8): 503–510, 1968.
24. E. Bahar, Fields in waveguide bends expressed in terms of coupled local annular waveguide modes, *IEEE Trans. Microw. Theory Tech.*, **MTT-17** (4): 210–217, 1969.
25. E. Bahar, G. Govindarajan, Rectangular and annular modal analyses of multimode waveguide bends, *IEEE Trans. Microw. Theory Tech.*, **MTT-21** (15): 819–824, 1973.
26. S. W. Maley, E. Bahar, Effects of wall perturbations in multimode waveguides, *J. Res. Natl. Bur. Stand.*, **68D** (1): 35–42, 1964.
27. E. Bahar, Computations of mode scattering coefficients due to ionospheric perturbation and comparison with VLF radio measurements, *Proc. Inst. Electr. Eng.*, **117** (4): 735–738, 1970.
28. E. Bahar, G. Crain, Synthesis of multimode waveguide transition sections, *Proc. Inst. Electr.Eng.*, **115** (10): 1395–1397, 1968.
29. E. Bahar, J. R. Wait, Propagation in a model terrestrial waveguide of nonuniform height, theory and experiment, *J. Res. Natl. Bur. Stand.*, **69D** (11): 1445–1463, 1965.
30. E. Bahar, Propagation of VLF radio waves in a model earth ionosphere waveguide of arbitrary height and finite surface impedance boundary: Theory and experiment, *Radio Sci.*, **1** (8): 925–938, 1966.
31. E. Bahar, J. R. Wait, Microwave model techniques to study VLF radio propagation in the earth ionosphere waveguide, in J. Fox (ed.), *Quasi-Optics*, New York: Interscience, 1964, pp. 447–464.
32. E. Bahar, Propagation in a microwave model waveguide of variable surface impedance: Theory and experiment, *IEEE Trans. Microw. Theory Tech.*, **MTT-14** (11): 572–578, 1966.
33. E. Bahar, Analysis of mode conversion in waveguide transition section with surface impedance boundaries applied to VLF radio propagation, *IEEE Trans. Antennas Propag.*, **AP-16** (6): 673–678, 1968.
34. J. R. Wait, E. Bahar, Simulation of curvature in a straight model waveguide, *Electron. Lett.*, **2** (10): 358, 1966.
35. E. Bahar, Scattering of VLF radio waves in the curved earth ionosphere waveguide, *Radio Sci.*, **3** (2): 145–154, 1968.
36. E. Bahar, Inhomogeneous dielectric filling in a straight model waveguide to simulate curvature of waveguide boundaries, *Proc. Inst. Electr. Eng.*, **116** (1): 84–86, 1969.
37. D. E. Kerr, *Propagation of Short Radio Waves*, MIT Radiat. Lab. Ser. 13, New York: McGraw-Hill, 1951.
38. E. Bahar, Radio wave propagation over a rough, variable impedance, boundary, Part I. Full wave analysis, *IEEE Trans. Antennas Propag.*, **AP-20** (3): 354–362, 1972.
39. E. Bahar, Radio wave propagation over a rough, variable impedance, boundary, Part II. Full wave analysis, *IEEE Trans. Antennas Propag.*, **AP-20** (3): 362–368, 1972.
40. G. A. Schlak, J. R. Wait, Electromagnetic wave propagation over a nonparallel stratified conducting medium, *Can. J. Phys.*, **45**: 3697–3720, 1967.
41. M. J. Kontorowich, N. M. Lebedev, Kontorowich Lebedev Transforms, Academy of Science USSR, *J. Phys.*, **1**: 229–241, 1939.
42. E. Bahar, Generalized Bessel transform and its relationship to the Fourier, Watson and Kontorowich–Lebedev transforms, *J. Math. Phys.*, **12** (2): 179–185, 1971.
43. R. J. King, C. H. Husting, Microwave surface impedance measurements of a dielectric wedge on a perfect conductor, *Can. J. Phys.*, **49**: 820–830, 1971.
44. E. Bahar, Generalized Fourier transform for stratified media, *Can. J. Phys.*, **50** (24): 3123–3131, 1972.
45. E. Bahar, Radio wave propagation in stratified media with nonuniform boundaries and varying electromagnetic parameters—Full wave analysis, *Can. J. Phys.*, **50** (24): 3132–3142, 1972.
46. E. Bahar, Electromagnetic wave propagation in inhomogeneous multilayered structures of arbitrary thickness—Generalized field transforms, *J. Math. Phys.*, **14** (8): 1024–1029, 1973.

47. E. Bahar, Electromagnetic wave propagation in inhomogeneous multilayered structures of arbitrary thickness—Full wave solutions, *J. Math. Phys.*, **14** (8): 1030–1036, 1973.
48. E. Bahar, Generalized WKB method with applications to problems of propagation in nonhomogeneous media, *J. Math. Phys.*, **8** (9): 1735–1746, 1967.
49. E. Bahar, Propagation of radio waves over a nonuniform layered medium, *Radio Sci.*, **5** (7): 1069–1076, 1970.
50. E. Bahar, Radiation from layered structures of variable thickness, *Radio Sci.*, **6** (12): 1109–1116, 1971.
51. E. Bahar, Radiation by a line source over nonuniform stratified earth (with G. Govindarajan), *J. Geophys. Res.*, **78** (2): 393–406, 1973.
52. E. Bahar, Radio wave propagation in nonuniform multilayered cylindrical structures—Generalized field transforms, *J. Math. Phys.*, **15** (11): 1977–1981, 1974.
53. E. Bahar, Radio wave propagation in nonuniform multilayered cylindrical structures—Full wave solutions, *J. Math. Phys.*, **15** (11): 1982–1986, 1974.
54. E. Bahar, Field transforms for multilayered cylindrical and spherical structures of finite conductivity, *Can. J. Phys.*, **53** (11): 1078–1087, 1975.
55. E. Bahar, Propagation in irregular multilayered cylindrical structures of finite conductivity—Full wave solutions, *Can. J. Phys.*, **53** (11): 1088–1096, 1975.
56. E. Bahar, Electromagnetic waves in irregular multilayered spheroidal structures of finite conductivity–Full wave solutions, *Radio Sci.*, **11** (2): 137–147, 1976.
57. E. Bahar, Computations of the transmission and reflection scattering coefficients in an irregular spheroidal model of the earth-ionosphere waveguide, *Radio Sci.*, **15** (5): 987–1000, 1980.
58. E. Bahar, Radio waves in an irregular spheroidal model of the erath ionosphere waveguide (with M. A. Fitzwater), *IEEE Trans. Antennas Propag.*, **AP-28** (4): 591–592, 1980.
59. J. R. Wait, *Waves in Stratified Media*, New York: Macmillan, 1962.
60. E. Bahar, M. A. Fitzwater, Numerical technique to trace the loci of the complex roots of characteristic equations in mathematical physics, *SIAM J. Sci. Stat. Comput.*, **2** (4): 389–403, 1981.
61. R. E. Collin, Electromagnetic scattering from perfectly conducting rough surfaces (a new full wave method), *IEEE Trans. Antennas Propag.*, **AP-40** (12): 1416–1477, 1992.
62. E. Bahar, Full wave solutions for the depolarization of the scattered radiation fields by rough surfaces of arbitrary slope, *IEEE Trans. Antennas Propag.*, **AP-29** (3): 443–454, 1981.
63. M. L. Sancer, Shadow corrected electromagnetic scattering from randomly rough surface, *IEEE Trans. Antennas Propag.*, **AP-17**: 577–585, 1969.
64. E. Bahar, B. S. Lee, Radar scatter cross sections for two dimensional random rough surfaces—Full wave solutions and comparisons with experiments, *Waves Random Media*, **6**: 1–23, 1996.
65. E. Bahar, Scattering cross sections for composite random surfaces—Full wave analysis, *Radio Sci.*, **16** (6): 1327–1335, 1981.
66. E. Bahar, Y. Zhang, A new unified full wave approach to evaluate the scatter cross sections of composite random rough surfaces, *IEEE Trans. Geosci. Remote Sens.*, **34** (4): 973–980, 1996.
67. E. Bahar, Y. Zhang, Numerical solutions for the scattered fields from rough surfaces using the full wave generalized telegraphists' equations, *Int. J. Numer. Model.*, **10**: 83–99, 1997.
68. E. Bahar, Excitation of lateral waves and the scattered radiation fields by rough surfaces of arbitrary slope, *Radio Sci.*, **15** (6): 1095–1104, 1980.
69. E. Bahar, Excitation of surface waves and the scattered radiation fields by rough surfaces of arbitrary slope, *IEEE Trans. Microw. Theory Tech.*, **MTT-28** (9): 999–1006, 1980.
70. E. Bahar, B. S. Lee, Transmission scatter cross sections across two-dimensional random rough surfaces—Full wave solutions and comparison with numerical results, *Waves Random Media*, **6**: 25–48, 1996.
71. E. Bahar, Physical interpretation of the full wave solutions for the electromagnetic fields scattered from irregular stratified media, *Radio Sci.*, **23** (5): 749–759, 1988.
72. S. M. Haugland, Scattering of electromagnetic waves from coated rough surfaces full wave approach, Thesis, University of Nebraska—Lincoln, 1991.
73. E. Bahar, S. M. Haugland, A. H. Carrieri, Full wave solutions for Mueller matrix elements used to remotely sense irregular stratified structures, *Proc. IGARSS '91 Remote Sens.: Global Monit. Earth Manage.*, Espoo, Finland, Vol. 1, 1991, pp. 1479–1482.

74. S. M. Haugland, E. Bahar, A. H. Carrieri, Identification of contaminant coatings over rough surfaces using polarized IR scattering, *Appl. Opt.*, **31** (19): 3847–3852, 1992.
75. E. Bahar, M. Fitzwater, Full wave physical models of nonspecular scattering in irregular stratified media, *IEEE Trans. Antennas Propag.*, **AP-S 37** (12): 1609–1616, 1989.
76. R. D. Kubik, E. Bahar, Electromagnetic fields scattered from irregular layered media, *J. Opt. Soc. Amer. A*, **13** (10): 2050–2059, 1993.
77. E. Bahar, Full wave-co-polarized non specular transmission and reflection scattering matrix elements for rough surfaces, *J. Opt. Soc. Amer. A*, **5**: 1873–1882, 1988.
78. R. D. Kubik, E. Bahar, Radar polarimetry applied to scattering from irregular layered media, *J. Opt. Soc. Amer. A*, **15**: 2060–2071, 1996.

EZEKIEL BAHAR
University of Nebraska-Lincoln